2008

Persistence of defects during class-A sheet thermoforming of thermoplastic olefins

Jonathan Marmillo
Lehigh University

Marmillo, Jonathan

Persistence of Defects During Class-A Sheet Thermoforming of Thermoplastic Olefins

January 2009

Persistence of Defects During Class-A Sheet Thermoforming of Thermoplastic Olefins

by

Jonathan Marmillo

A Thesis

Presented to the Graduate and Research Committee

of Lehigh University

in Candidacy for the Degree of

Master of Science

in

Mechanical Engineering

Lehigh University

December 2008

This thesis is accepted and approved in partial fulfillment of the requirements for the Master of Science.

Dec. 5, 2008
Date

Thesis Advisor

Chairperson of Department

Acknowledgements:

I would like to thank my advisor Dr. Herman F. Nied for the opportunity to conduct my graduate research on one of his ongoing research projects in the field of thermoforming where there is still much to be learned. His guidance and advice were crucial to the completion of my work and I am infinitely appreciative for the countless hours he dedicated to helping me further my education.

My appreciation is also extended to Ph.D. student Burak Bekisli who brought me up to speed on the project at hand and greatly aided in my understanding of the thermoforming process.

Thanks to our project sponsor, Ford Motor Company, and specifically Kedzie Fernholz, for providing us with this interesting project and the means by which to investigate it.

Additionally, I want to recognize Dick Towne, Mechanical Engineering Shop Coordinator. Without his help the numerous design plans I made during the project couldn't have been constructed.

Finally, I would like to thank my family for their unconditional support and constant positive encouragement during the entire M.S. process.

Table of Contents:

List of Figures:

1. Abstract:

Modern thermoforming is a manufacturing operation that processes polymeric materials into parts used in everyday life. The process consists of numerous steps including heating a polymer, forming it with vacuum, then cooling and trimming it. However, it is not perfected and defects still occur during this manufacturing process.

Due to their low cost and weight, and relatively easy formability, plastics are becoming increasingly more used in the automotive field. The parts with high surface finish quality (Class-A Parts) are typically injection molded, however Ford has invested in research to produce these parts using thermoforming.

A research project was developed by Lehigh University and Ford Motor Co. to perform an analysis on the characteristics and causes of surface defects seen on two brands of Thermoplastic Olefins (TPO) which are used for Class-A exterior automotive parts. The material properties of the two polymers (Basell's Hifax® 756T and A. Schulman's Polytrope® TPP 1040E) were characterized using techniques including Dynamic Mechanical Analysis (DMA) and Differential Scanning Calorimetry (DSC). DSC data for the two polymers was similar but the DMA data showed that the Schulman 1040E had a higher modulus of elasticity in a temperature range of 40°C to 170°C. A thermoformed rocker panel produced at Ford's labs was scanned using an optical profilometer and shown to have a "valley" defect of 64.6 μm maximum depth. In an effort to simulate defect formation, material properties were input into ANSYS finite element simulation software to model defects related to the sheet sag behavior. However, it appears that global FEM simulation does not offer sufficient "resolution" to adequately

capture the detailed formation of microscopic defects without incorporating additional process physics.

For example, it is hypothesized that minute amounts of air trapped between the plastic and the mold can be a leading cause of microscopic defects. Sheets of TPO were thermoformed onto different mold configurations in an attempt to quantify trapped defects. The experiments trapped miniscule pockets of air, which then formed bubbles due to the pressure increase that results from increasing temperature. After the hot plastic (~215°C) heats the trapped air (initially at room temperature) the heat transferred to the air causes a significant pressure increase since this air is assumed to remain at a constant volume. Calculations show that air bubbles are formed with a pressure of ~23 psi (158580 Pa). The combination of a set temperature and pressure will have different effects on polymers with different viscoelastic properties. If a polymer's modulus increases at a faster rate when cooling it becomes stiffer faster. This higher modulus may be high enough so that the effects of pressure from an air bubble do not impact the final surface quality of a part.

2. Basic Concept of Thermoforming

2.1 Introduction

Since the commercialization of thermoplastic materials, thermoforming has rapidly become one of the fastest growing plastic manufacturing methods. This can be credited to the process' adaptability, low initial investment, speed, and ease of repetition. Thermoforming has taken the place of many other processes and has even allowed plastic parts to be used in applications where once metals dominated. It is used to manufacture many everyday items including car front door claddings and the general theory of this

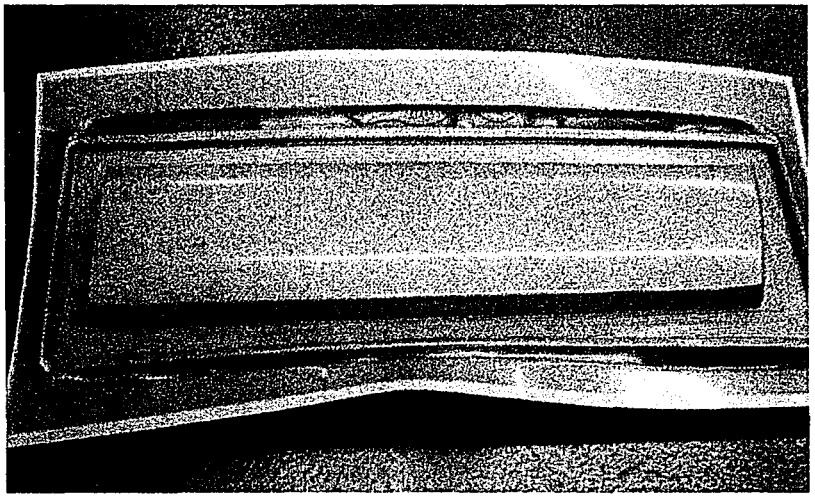

Figure 1: Front Door Cladding After Thermoforming [6]

manufacturing technique is fairly simple. A polymer sheet is heated in an oven above its glass transition temperature so it is softer and displays viscoelastic properties. The sheet is then positioned over a mold and a vacuum is applied so the plastic is fit tightly against the mold. After cooling, the mold is then removed leaving the formed part exposed so it can be trimmed to its final product.

2.2 History of Thermoforming

The earliest forms of thermoforming can be seen as far back as the early Egyptians who discovered that Keratin, a chemical in tortoise shells, could be heated so it was malleable and then draped over a form and cooled to produce containers to hold food. The Native Americans also found that cellulose, a component of tree bark, could be formed in the same way. [1,2] However, the process gained greater popularity around World War Two with the development of thermoplastics. Aircraft canopies, turrets, and relief maps were some products mass produced during the war and after it ended the process branched away from military applications and became much more commercially based. By the 1950's production levels were already high and equipment was being manufactured that continued to improve cycle time and repeatability. In the 1960's thermoforming branched into the packing industry (especially single serving foods) and the sign and appliance industries. [1,2]

By the 1970's high-speed machines were now being demanded by industry. Machines were being produced that could make 100,000 thermoformed parts per hour. At these high rates the amounts of scrap plastic that was being produced was extreme and methods were developed for recycling or reusing the leftover product. Since the machines were operating at much higher speeds the process controls needed to be improved and electronic and computer controls emerged onto the scene. [1,2] In the 1980's machines that started with simple plastic resin pellets and formed them into sheets where were then fed into the thermoformer emerged, and were called "pellet-to-product". In the 1990's the sluggish world economy slowed thermoformer purchasing and environmental concerns shook the industry. Much of the fast food industry stopped

serving take out food in thermoformed packages and numerous smaller companies were forced to close. However, in the past decade the industry has rebounded and technological advances have been made. More computerization has occurred introducing more precise control and higher quality products. However, this has reduced the number of thermoforming blue-collar manufacturing jobs since computers can now automate much of the process. [1,2]

2.3 Products Made / Industry Profile

Thermoformed parts extend into almost every industry and a short list showing the wide range of products should be mentioned. They include blister packs (medicine packages), take out/storage food containers, interior/exterior automotive parts, signs, refrigerator door liners, food serving trays, disposable plates, various presterilized surgical equipment, seedling plant trays, boat hulls, bathtubs, suitcase body frames, and even many types of coffins to name just a few.

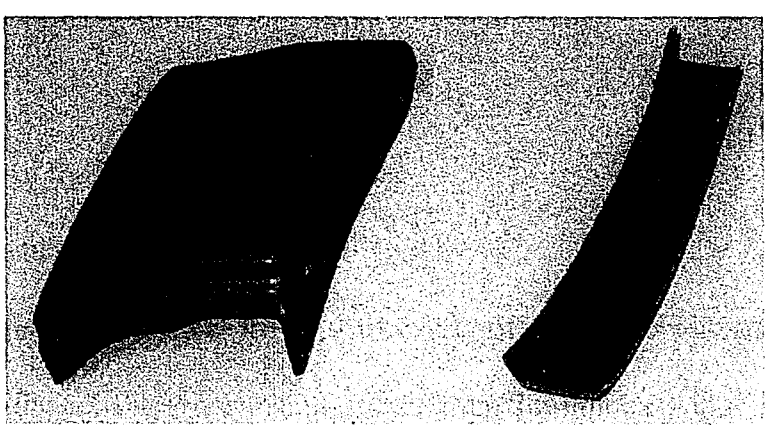

Figure 2: Two Automotive Exterior Body Parts Made By Thermoforming

The thermoforming industry has expanded rapidly since its inception and has become a worldwide business estimated at over 10 billion US dollars in sales annually

and it is estimated to be growing at a rate of 6% a year. [7] The industry is generally broken up into two sections, thin gauge (.060 inches or 1.5 mm and thinner) and thick or heavy gauge (.120 inches or 3 mm and thicker). [1] There is a small, but growing medium market for thicknesses in between the two previously mentioned thicknesses. In the North American market, the ratio of sales is about 25% thick gauge and 75% thin gauge. In 2003 it was reported there were about 150 thin gauge thermoforming companies in North America. Sixty percent formed proprietary products, thirty percent were custom formers, and ten percent were OEM companies with in-house thermoforming capabilities. About 250 heavy gauge thermoforming companies exist and the majority are custom product formers. [7] Production plants have grown from small shops to large sophisticated high volume and quality companies with multiple locations that are now in competition with domestic companies. This competition however has slowed the evolution of the manufacturing science since many companies have adopted the '"trade-secret" method of production and refuse to share technological advances with the industry as a whole in order to maintain a competitive edge.

3. Components of the Thermoforming Process

3.1. Thermoplastic Sheets

Thermoforming is able to exist because of the development of polymeric materials. Plastic polymers are manufactured from low molecular weight monomers molecules that are obtained after distillation from crude oil, coal, and natural gas. The monomers then undergo chemical processes (addition and condensation reactions) with catalysts, high temperature and pressure and form into thermoplastics or thermosets

which are long chain, high molecular weight molecules. Thermosets, once the resin has cured, cannot be reshaped and are generally not used for thermoforming. Thermoplastics however, can be reformed into new shapes when heated and are the primary material used for thermoforming. Most applications desire thermoplastics with high molecular weights (long molecule chains) so the chains can stretch longer distances when heated without failure, thus allowing higher strain in the product. [1]

The plastic needs to be fed into the thermoforming machines and this is done in two distinct fashions. These are either continuous sheets which are rolled around a spool or precut panels, both available in numerous combinations of thickness and width. Three basic methods are used and they are calendaring, casting, and extruding. All involve the addition of heat to the plastic resin and then reforming it into the desired shape. The most common is extrusion where plastic pellets are converted into a melt flow and forced through a die system and then cooled and cut into sheets or wound around a spool.

Depending on the application for which a part is being manufactured, specific material properties will be desired and thus the thermoplastic sheet selection process will be unique since each polymer exhibits different mechanical properties. During the sheet manufacturing process additives can be blended into the mix that can change color and modify material properties. Pigments can be added to create solid colors, or tints can be added to create a colored translucent effect both having minimal effects on material properties. Patterns can be printed on for decorative purposes and the automotive industry is now painting their rocker panel thermoforming stock before forming, reducing the need to paint it after manufacturing and thus saving money. However this will alter material properties so the process may need to be updated to accommodate for this.

Aluminum foil lined thermoplastics are being experimented with and plastics with composite fibers in them are rapidly gaining popularity. For more specialized material requirements laminates can be used. For example for UV and chemical resistance a layer of PMMA is put onto ABS, or for a flame retardant barrier PVC can be layered onto PMMA. [1] Common materials used in thermoforming applications are polypropylene (PP), polystyrene (PS), Polyvinyl Chloride (PVC), Low Density and High Density Polyethylene (LDPE, HDPE), Cellulose Acetate, Polymethylmethacrylate (PMMA), Acrylonitrile-Butadiene-Styrene (ABS), and ThermoPlastic Olefin (TPO). Each will have different forming temperatures and different properties suited to an application so care must be taken when selecting a polymer for thermoforming. Typical forming ranges for numerous polymers can be seen in Figure 3.

Plastic	Temperature Range °C
LDPE	470-630
HDPE	510-630
PS	510-630
PVC	530-630
PMMA	530-630
PET	605-630
Cellulose acetate	210-255

Figure 3: Typical Forming Ranges for Several Thermoformable Plastics [1]

There are numerous books dedicated to these properties such as the Polymer Blends Handbook Vol 1-2 by L. A. Utracki [13] can be extremely helpful in this process.

3.2. Clamping Systems

With the proper material selected, the next step in the process is to securely clamp sheets of the polymer in the machine on all four sides. If all four sides are not properly

clamped material may slip and pull away from the clamping area causing an undesirable thickness distribution in the finished part. Numerous methods are available and depend greatly on machine type. For small single part machines a manual clamp frame is a common choice. The sheet stock is placed inside the frame and the user clamps it closed and a security latch is then activated for additional clamping pressure. Some clamps have grooves and spikes on opposite sides of the frame allowing the clamp to grip the sheet better. Lehigh's ZMD HD-300 Series thermoforming machine has a clamp frame, which secures the sheet on all four sides with pressure and gripping spikes and it is pneumatically activated allowing greater pressure for clamping.

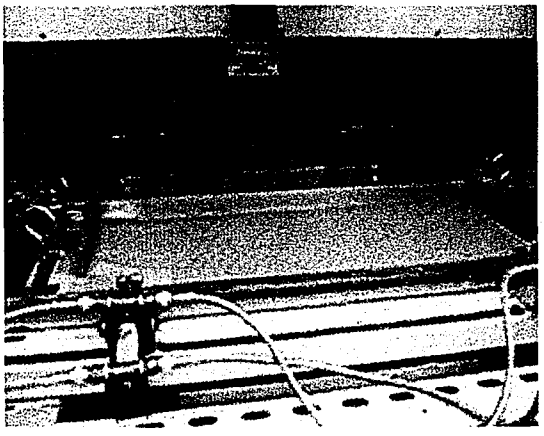

Figure 4: Lehigh's ZMD HD-300 Thermoformer's Clamping System

This type of system is common on small commercial thick gauge forming machines, however the process of positioning the sheets on the frame is automated by robotic arms for increased productivity.

Thin gauge thermoformers typically are roll-fed, and called continuous sheet formers. Clamping is achieved by parallel continuous loop chain-fed pins that penetrate

the sheet at small intervals near the edge of the roll stock. Although the chains are only on two sides of the material the continuity of the web can act as the other two sides of the

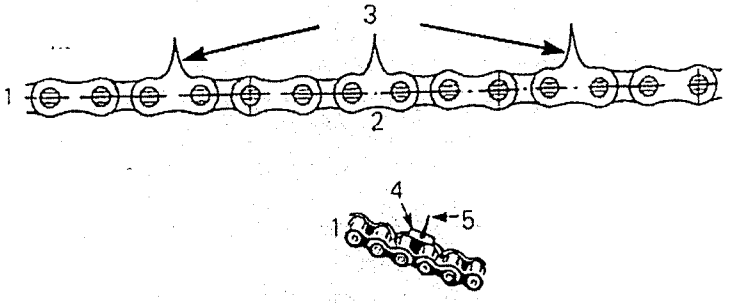

Figure 5: Sheet Transport Chains: (1) Roller Chain, (2) Standard Chain Link, (3) One Piece Pin Link, (4) Flanged Link, (5) Riveted Pin [2]

clamp sufficiently. If additional support is needed on the two sides perpendicular to the chains then individual clamp bars can be installed and greatly reduce any distortion. This chain system will then guide the sheet along its path through the rest of the machine.

3.3 Heating Systems

Heating of the plastic sheet is a critical part of thermoforming. Heat applied can come from many different sources, but must be identical for every cycle to ensure part uniformity. Up to 80% of the total energy needed for the entire thermoforming process in consumed during this heating phase and consideration must be made to reduce excess energy consumption in this phase. [2]

Gas-fired convection ovens are commonly used for heating of extra large panels and extra thick gauges by means of hot air convection. This is a cost effective solution for parts with extra long heating cycle times since gas is less expensive than electricity.

Although the control is not as great as with electric heating methods, temperature control is not as critical for these extra large parts.

Contact heating is an older method that involves touching the sheet to a hot, usually metal, plate and is not commonly seen anymore.

Radiant heating uses infrared light spectrum wavelengths to heat the surface of the material. Then the heat is dissipated through the body of the polymer by conduction. If the material is translucent some radiation may pass through the material but will then be redirected back at it through the use of reflective shields behind the IR lamps. The IR spectrum ranges from 1.2 microns to 8 microns but the best conversion efficiency from electrical power to radiant energy is around the wavelengths of 3-3.5 microns. [2]

Some of the newest and most cost effective radiant heaters are catalytic infrared heaters. Gas and air is fed into an enclosed chamber that is at a pre-elevated temperature via small tubing. In the chambers is a catalyst, typically platinum shavings, which triggers oxidation of the gas without burning. This generates infrared heat that heats the sheet. These emit longer wavelengths and should only be used for applications where a uniform temperature distribution is desired. [1-2]

Infrared radiation heaters are common in the electric form, see Figure 6. Their cores are made of a high resistance wire (nickel-chrome alloy wire) and when electricity is run through the wire, the resistance makes it glow red hot. Many varieties exist including tubular or rod heaters which are coiled wire enclosed in a steel tube jacket. The jacket is filled with insulating material under pressure and sealed and terminal ends applied. The heat from the wire makes the entire tube hot which will heat up the sheets.

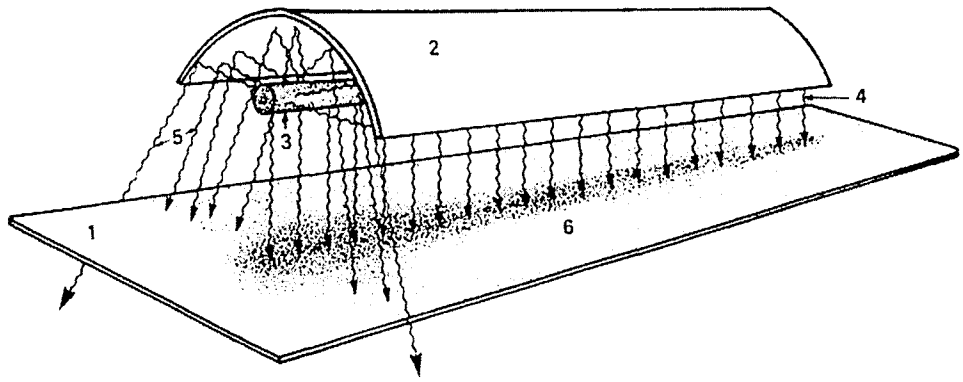

Figure 6: Reflectorized Radiant Heater Source: (1) Thermoplastic Sheet, (2) Reflector, (3) Heating Element, (4) Direct Heat, (5) Reflected Heat, (6) Heat Distribution on Sheet [2]

IR heaters come in many lengths, wattages and all common voltages which can be arranged into a custom array to provide various heating patterns. [2]

Ceramic heaters are also very common ways of heating. Though they are more expensive than the tubular type, the benefit of greater temperature controllability can outweigh the cost disadvantage. Ceramic plates are made with coiled heating element wires embedded in them and then glazed over. When current is passed through the wires they glow red hot causing in turn the ceramic unit to glow red hot and the entire unit emits radiant energy. Units come in various sizes and are installed into thermoforming machines in rows and columns. Their output can easily be controlled by computers which makes it easy to obtain various heating patterns.

Quartz heater popularity is on the rise because of its high efficiency. For these heaters quartz is manufactured in a tubular shape and the nickel-chrome wire is threaded through the core. The ends are fitted with porcelain caps with leads which also act as insulators at the ends. Because quartz will not interfere with the infrared wavelengths it can be turned on and off between cycles instantly saving small amounts of energy each

cycle which then adds up to a great deal of energy savings. A flat plate variety of quartz heaters also exits. [2]

Heat transfer from the heating elements to the sheet can happen in three ways: conduction, convection and radiation. The time dependent net energy increase or decrease equals the change in heat flux within the plastic sheet.

$$\frac{\partial H}{\partial \theta} \approx \rho c_p \frac{\partial T}{\partial \theta} = \frac{\partial}{\partial x}(k\frac{\partial T}{\partial x}) = \frac{\partial}{\partial x}(\frac{Q}{A}) \qquad (1)$$

Where: H = Enthalpy, T = Temperature, ρ = Density, θ = Time, c_p = Heat Capacity, k = Thermal Conductivity, Q/A = Heat Flux. [1]

The temperature is now a function of time and position across the thickness of the sheet, $T(\theta,x)$.

To solve this equation three boundary conditions are needed:

The initial condition which is the initial temperature throughout the sheet and this can assumed to be uniform through the thickness so:

$$T(0,L)=T_O \qquad (2)$$

L is the half sheet thickness for equal two sided energy flux into the sheet surface. [1]

The symmetry condition is needed and if the sheet is headed uniformly on both sides the centerline forms a plane of symmetry and thus the heat flux at the symmetry plane is zero. [1]

$$\left.\frac{dT}{dx}\right|_{\theta,x=0} = 0 \qquad (3)$$

The surface condition is the third condition needed. Conduction is solid phase contact heat transfer and the thermal properties of the sheet discussed earlier are very important. At the surface this will be

$$T(\theta,x=L) = T_L(\theta) \tag{4}$$

$T_L(\theta)$ can be time dependent or constant, θ is time and x=L is the surface location. [1]

Convection occurs when the sheet is in contact with a fluid environment and is:

$$\left.\frac{Q}{A}\right|_{\Theta,x=L} = -k\left.\frac{dT}{dx}\right|_{\Theta,x=L} = h[T(\Theta - T_\infty(\Theta)] \tag{5}$$

Where h is the convective heat transfer coefficient (10 to 100 W/m^2 for air), $T(\theta)$ is the sheet surface temperature and $T_\infty(\theta)$ is the temperature of the environment.

Radiation is the third type of heat transfer and the equation is:

$$\left.\frac{Q}{A}\right|_{\Theta,x=L} = G[T^4 - T_\infty(\Theta)] \tag{6}$$

Where G is a factor including geometry and radiation characteristics of both the heating source and the sheet. [1]

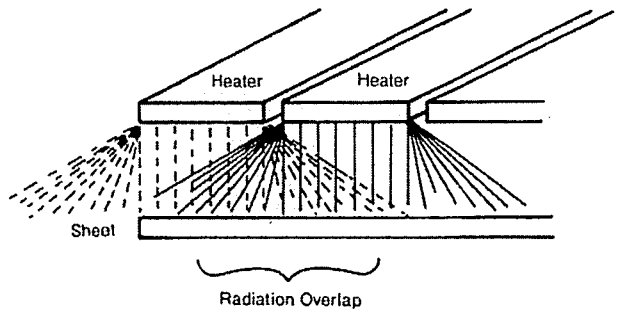

Figure 7: Schematic of Radiation Overlap From Heaters to Sheet [1]

With these three boundary conditions the polymer temperature as a function of time and position can be solved for.

The amount of energy received by a single plastic element from all heaters can be calculated as:

$$q_{\Sigma 1 \leftrightarrow 2} = \sigma F_g [\sum_{A1} \frac{z^2}{\pi (x^2 + y^2 + z^2)^2} (T_{heater}^4 - T_{sheet}^4) \Delta A1 \Delta A2 \qquad (7)$$

Where: A1 is the heater element area and A2 is the plastic sheet area, F_G is the gray body correction factor for radiation, σ is the Stephan Boltzman constant, and a grid is created of elements in the x-y direction separated by a distance z in the Z direction.

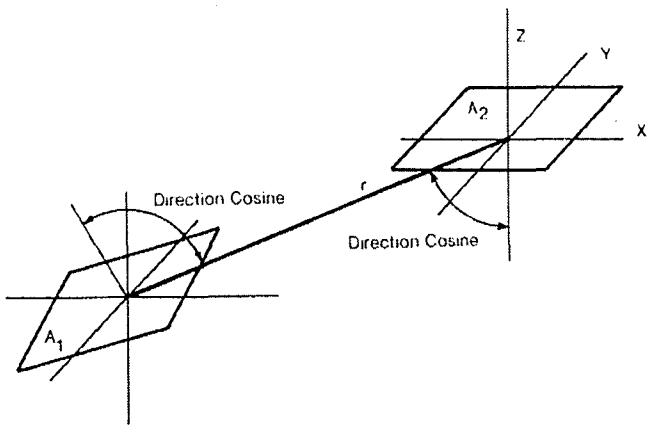

Figure 8: Radiation Ray Tracing Between Finite Parallel Plane Elements [1]

3.4. Molds

A mold is needed for the thermoplastic sheet to be formed and the material of choice for almost all molds is aluminum. It is lightweight, easily machined and has a high thermal conductivity, so heat from formed plastic can be easily removed and the sheet cooled. Plastic shrinkage should be compensated for when designing the mold size. Commercial molds today have internal tubing and are actively cooled. Coolant lines can

be drilled into the molds or positioned before casting. The following picture is a schematic showing a possible mold cooling system. [1,2]

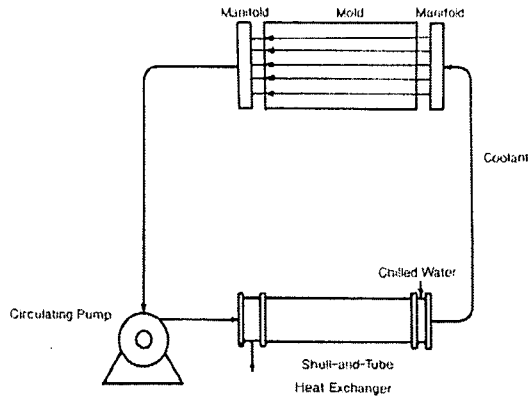

Figure 9: Example of a Mold Cooling System [1]

A vacuum is applied to ensure the polymer sheet fits tightly against the mold ensuring proper product dimensions. This means that the trapped air between the sheet and mold must be sucked out. Small holes are drilled into the mold surface and for ideal air removal should be placed along the corners, bottom and sidewall intersections, and into all critical geometries. Engraved patterns and lettering must have vent holes to ensure proper detail levels. The diameter and total number of holes must be meticulously calculated to ensure proper ventilation. If the vent hole diameter is too large plastic will be drawn into it causing defects. If it is too small or there are not enough holes the draw-down rate of the sheet will be a function of the air removal rate, which can cause the sheet to cool before it is in total contact with the mold. [1,2]

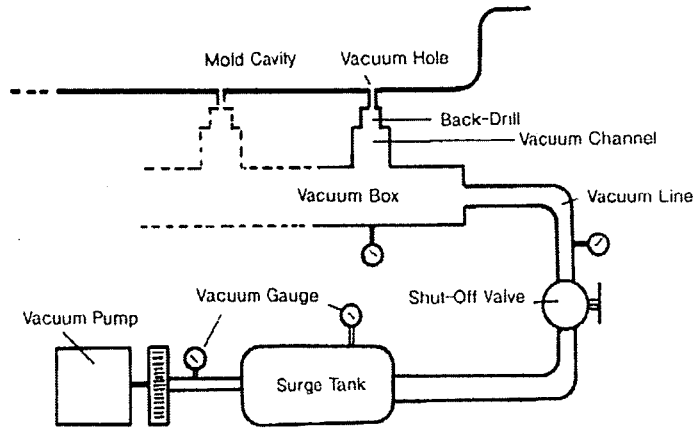

Figure 10: Typical Plumbing Between Mold Cavity and Vacuum Pump [1]

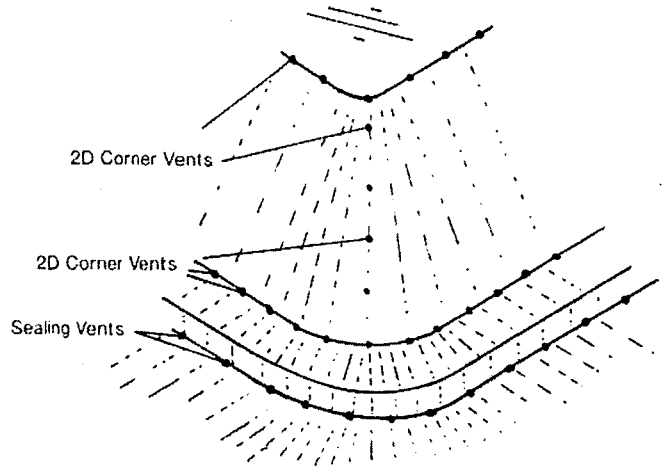

Figure 11: Vent Holes Located at Critical Points [1]

3.4.a Female vs Male Mold

There is an extremely large amount of variations on possible mold setups, but the two major categories are female and male molds.

Female molds are a mold made with a cavity and the heated sheet is forced into the cavity by either a vacuum or pressure from the outer side of the sheet or both. [2] For

a vacuum to be able to function properly a top box, called the pressure box, is lowered on an upper platen sealing the sheet in an air tight box. This type of mold always transfers any mold surface features onto the finished part. The part thickness decreases as the plastic is stretched down the sides of the mold and into the bottom. This is called the depth-of-draw ratio and the deeper the mold, the more surface area the plastic must cover, which means a reduction in part thickness. Plug assist (discussed later) can be added to this type of mold to decrease the depth-of-draw ratio and create a more uniform thickness distribution. Since the plastic will shrink after cooling, removal of parts from female molds is sometimes easier than removal from male molds. [1,2]

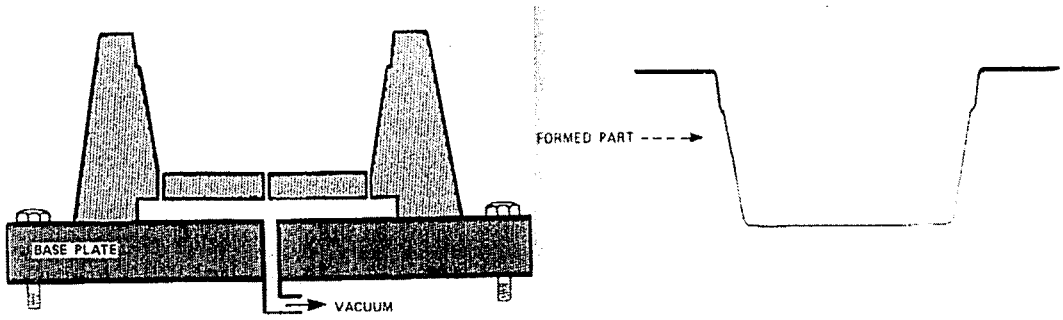

Figure 12A: Example of a Female Mold and Resulting Surface Thickness Distribution [2]

Male molds are molds that take the shape of a protrusion and are often used in manufacturing because they are easier to machine. The heated sheet is lowered onto the mold like a drape (or the mold which sits on a moveable platen is raised into the sheet) and a vacuum is applied after pressure box on a top platen is lowered to ensure it is airtight. The location where the plastic first touches the mold will remain the thickest part of the formed product and as the material is stretched down the sidewalls the thickness will decrease. Since the plastic will shrink as it cools, it tightens onto the mold.

To aid in the removal process pressurized air is sometimes blown through the separately drilled holes near the tip of the mold where it is strongest structurally. The existing vacuum holes are not used because the air will seek the path of least resistance, causing the thinnest parts to be blown off first, which will bend and not actually help the part in removal. [1,2]

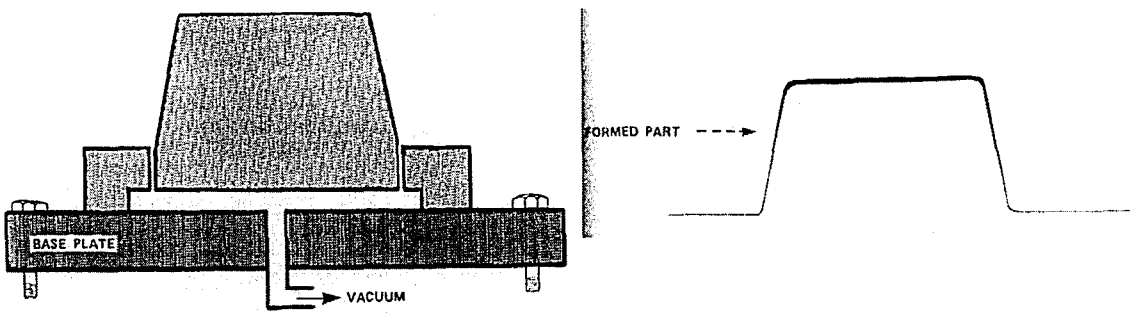

Figure 12 B: Example of a Male Mold and Resulting Surface Thickness Distribution [2]

The previously mentioned Plug Assist forming is the most commonly used Technique for deeper draw ratios. The plug is basically a much smaller similarly shaped part that would fit into the female mold. It is attached to another movable platen which is above the sheet. The platen is then lowered into the sheet stretching it and sealing it in a pressure box. The plug helps to stretch and push the sheet into female molds and draw ratios of 1:7 can even be achieved. It provides greatly improved material thickness distribution and with proper plug temperature, size, and motion a near uniform distribution can be attained. [2] The plug's temperature is usually slightly less that that of the heated sheet so when it makes contact with the sheet it will absorb some heat causing slight stiffening of the sheet. This stiffening will make the sheet less susceptible to stretching causing those areas to be thicker but this also means that the sidewalls can be unacceptably thin. To counteract this effect the plug is heated and held at the same

temperature as the heated sheet. Plugs can be made of many materials such as wood, plastic, but most commonly are aluminum as it is the easiest to control the temperature. The Figure 13 sequence shows the plug assist process which consists of sheet clamping, prestretching, forming, and mold opening and stripping. [1,2]

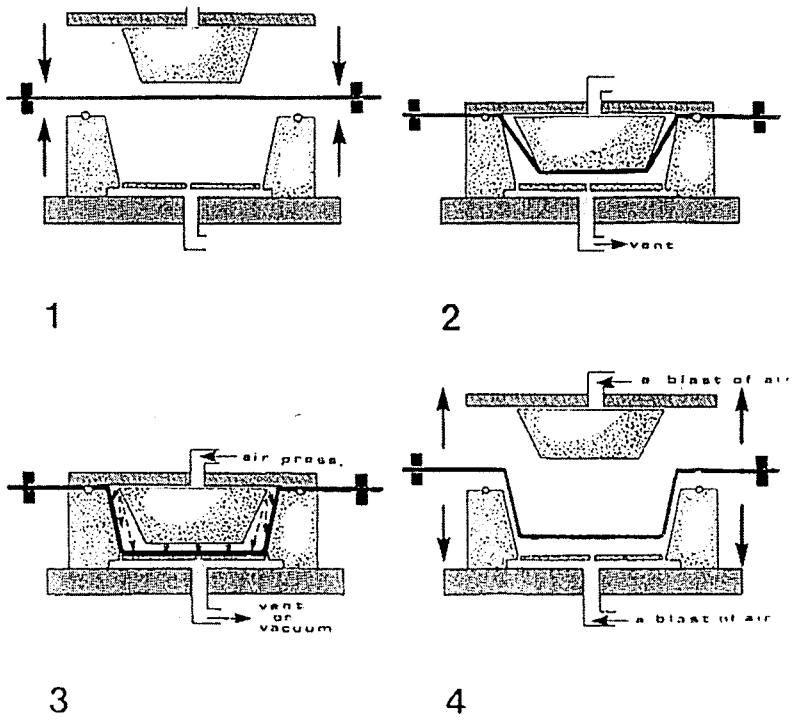

Figure 13: Plug Assist Thermoforming: (1) Sheet Clamping, (2) Prestretching, (3) Forming, (4), Mold Opening and Stripping [2]

Preblowing is a technique used on male molds that can have a similar effect as plug assist does for female molds. A pressure is applied to the underside of the sheet prestretching it and causing a bubble to form. The mold is then raised up into the bubble and the vacuum applied creating a more even thickness distribution.

A combination of these two techniques is called Pressure Bubble Plug-Assist Forming in which a bubble is formed on a sheet over a female mold. A plug is then pressed into the bubble and lowered into the mold and finally the vacuum is applied. The

result is a part with an extremely uniform thickness distribution. The Figure 14 illustrates the process.

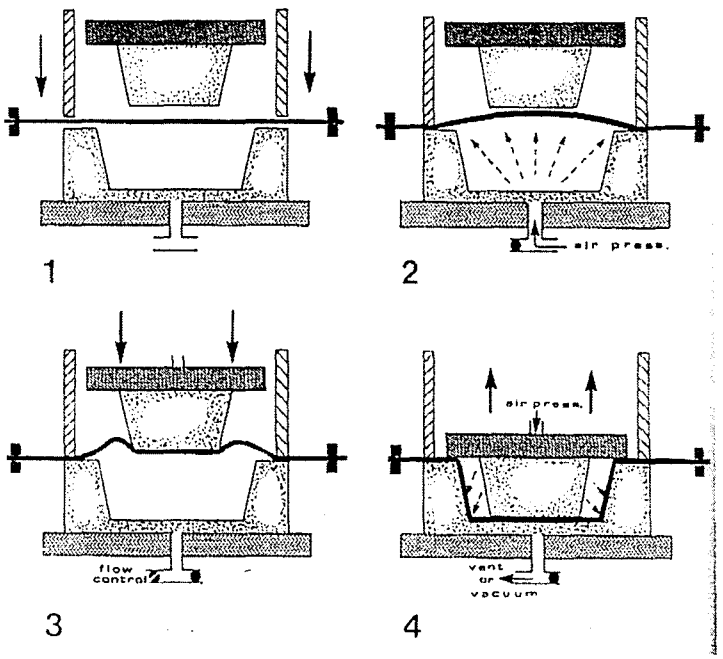

Figure 14: Pressure Bubble Plug-Assist Forming: (1) Preheat Sheet Clamping, (2) Prestretching of Sheet, (3) Mold Closing, (4) Pressure Forming Into Female Mold [2]

3.5. Cooling and Trimming

The formed part needs to be properly cooled or it will deform during the removal process. As mentioned before, modern commercial molds have coolant channels running through them to remove heat from the plastic and many machines have fans that blow air on the exposed side of the sheet to add convective heat removal. Once the part is below T_G and structurally stable it can be removed by backing out the mold or applying a pressure to the underside of the formed part to assist it in the removal process as mentioned earlier.

The part needs to be finished by cutting off the excess webbing plastic that is not wanted. This process can be performed by hand but in commercial machines is

automated often with the use of a die. After the part is formed a steel die is brought down in top of the product trimming it to the desired dimensions. This is known as trim-in-place, or in-situ, and saves time on the overall process cycle making it an ideal choice for manufactures. For more complex shapes the part can be moved onto a jig where a router will cut the part in an automated fashion. For extremely high speed cutting guided high power lasers can cut the part into any shape extremely accurately.[2] However, these also come with a higher price tag.

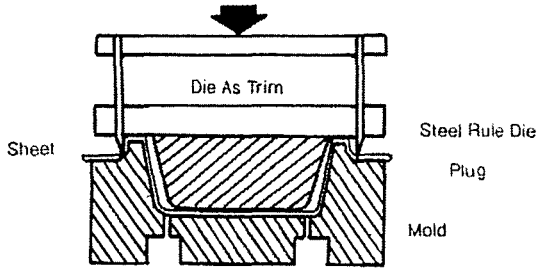

Figure 15: In-Situ Trimming Die Lowered to Cut Formed Part [2]

3.6. Limitations in Thermoforming

Many defects can occur during the thermoforming process, although with proper design they can be reduced or eliminated. "Webs are formed when the hot stretched plastic surface area in a local region is greater than the surface area of the mold in that region. Even though the plastic is considered to be an elastic rubbery solid, as the sheet is drawn toward the mold surface, certain sections of the sheet touch other sections before they touch the mold surface. When hot plastic touches hot plastic, the forces required to pull them apart are far greater than the force need to stretch surrounding plastic against the mold surface. As a result, a web is formed."[1] Plug assist and preblowing can reduce this effect but sometimes web catchers are needed. They are posts beyond the

critical area of the mold that catch the stretch so the web forms at their location instead of on the part itself. [1]

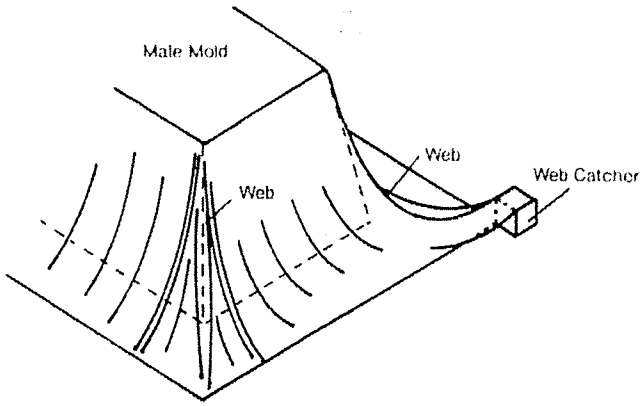

Figure 16: Web Formation and Web Catcher for Male Mold Forming [1]

Undercuts are another limitation of thermoforming and generally not desired when performing mold design. They can result in very thin corners and are more successful if radii are larger. An additional ejector plate that aids the undercut may be necessary to properly eject it without deformation.

Draft angles of the wall are necessary because right angled parts will result in extremely thin corners and in general no sharp edges should be included in mold design.

Ripples and other surface defects can occur if proper design is not considered. Improper sheet temperature or trapped bubbles could lead to these kinds of defects.

Depth-of-draw is another limitation. A general rule of thumb in the industry is that the ratio of the mold opening to the depth of the mold should not exceed 1:7.[2] However, with proper plug assist and preblowing larger ratios can be obtained with the tradeoff of a thinner part.

During the thermoforming process not all details that were present on the mold will be transferred to the finished part. However, with a highly polished mold and higher forming forces the detail transfer can be improved. Additionally, the side of plastic not touching the mold will show poor details. Thus if fine detail, such as imprinted lettering, is needed on the outside of the part it should be touching the mold surface. However, some sheets come pre-made with a desired exterior surface finish on one side of the sheet. This side should not touch the mold during forming, or the contact could cause a blemish thus ruining the desired exterior finish.

4. Observations of Defect Formation in TPO During Forming

As Ford Research and Development in Detroit, Michigan, experimented with the thermoforming of high surface finish quality (Class-A) parts defects became noticeable in some finished rocker panel parts. Ford was testing two polymers, one manufactured by Basell [12] and the other by A. Schulman [11], on their Geiss T8 thermoformer.[6] The sheets had a minimum thickness of 0.12" (3mm); this falls into thick sheet thermoforming, which could result in a significant temperature variation through the thickness while heating the sheet.

Sheets were inserted into the machine and heated to approximately 176°C (350°F) and then formed. "All edges of the sheet are clamped prior to heating cycle, restricting any movement of the sheet. The heat and increased temperature forces the sheet to extend and the clamped sheet can only find way to extend itself by forming bubbles or waves, in the out-of-plane direction. The concept is very similar to buckling."[6] While this is happening the sheet is also beginning to sag. To try and counter the sag

effect, Ford was using preblowing to keep the sheet at its initial height. Figure 17 illustrates the result of what the sheet looks like while all these forces are at work.

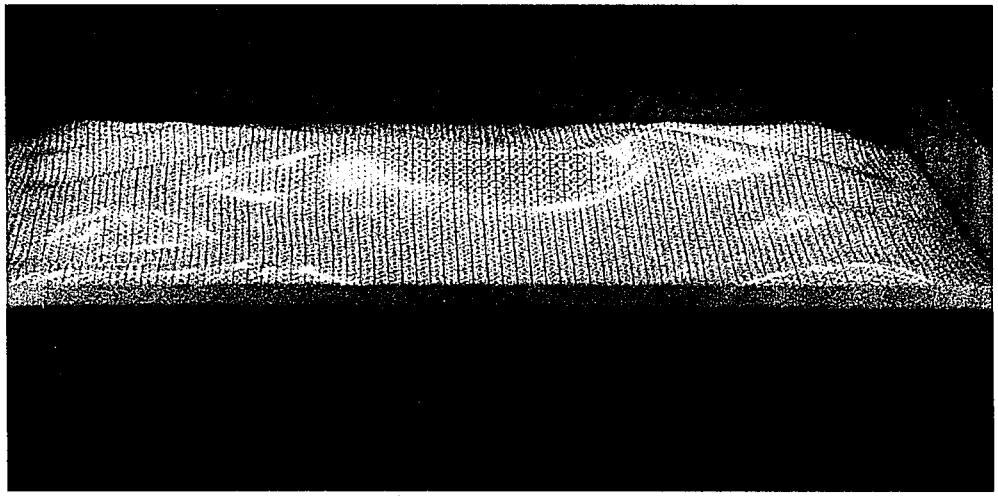

Figure 17: Deformation of TPO Sheet During Early Heating Stages, Prior to Forming of Rocker Panels [6]

> Thermoforming trials of these parts in the previous attempts had given inconsistent results, many times the surface quality of the finished product had been unacceptable. The surface defects can be classified in many different ways, but the term "waviness" is more common for the most defects. It is generally a continuous defect, in appearance of a straight line, starting from one corner up to another corner along the width. Moreover it is repeated after some distance along the length. The number of these defects on a part and the distance between two successive defects seem to be varying and the defects are more frequent for more slender, high aspect ratio parts. [6]

After part forming and cooling, they are inspected to see if visible defects exist, if so they are not Class-A and thus unusable. Of the two polymers tested, the Schulman 1040E consistently displaced the "waviness" defect while the Basell 756T displayed "almost consistently perfect looking parts with the same parameters used Schulman 1040E forming... and it is clear that some material properties are effective on this problem." [6]

Ford wished to know why the Basell 756T consistently formed with less defects and unformed sheet samples of both materials were sent to Lehigh University and a polymer characterization process was begun. Ford also sent Lehigh sample parts formed using Schulman 1040E containing a defect to quantify it and investigate the possible causes of the formation of defects.

4.1. Optical Profilometer

To better characterize the defects seen on Schulman 1040E samples provided by Ford R&D, a STIL Micromeasure Optical Profilometer was used to accurately measure the surface characteristics in the neighborhood of clearly identified defects. The machine, seen below, consists of an optical sensor, a computer controlled moving platform on which the sample rests, a control pad to position the platform, and electronic controls that analyzes the data that is displayed on a computer.

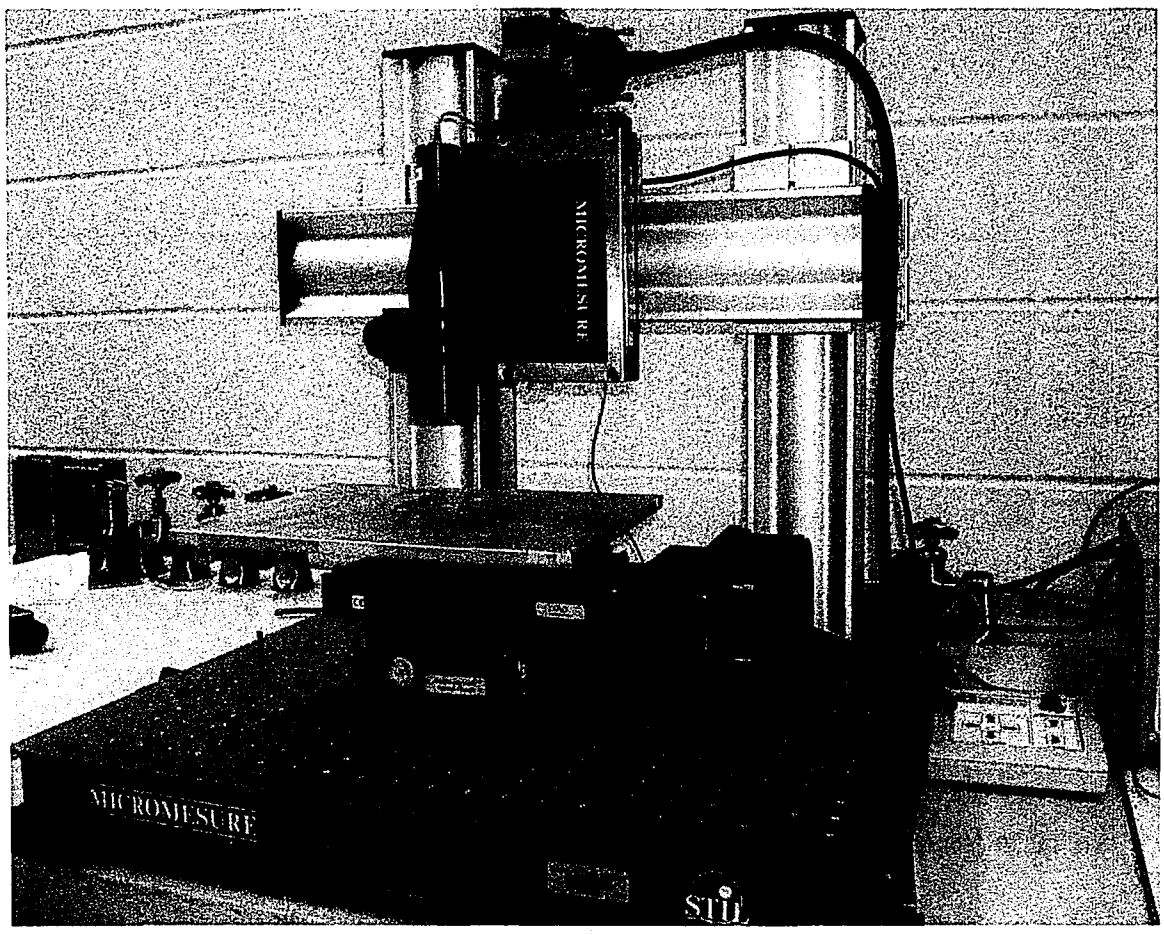

Figure 18: Lehigh's Optical Profilometer

The system has three interchangeable optical sensors whose specifics are listed below:

Sensor Number	2	0	1
Z Measurement Range	350 µm	3 mm	10 mm
Z Resolution (nm)	10	100	300
Z Accuracy (nm)	60	600	900
Working Distance (mm)	12.7	26.9	66.9
Spot Diameter (µm)	5.2	25	51
Lateral Resolution (µm)	2.6	12.5	25.5
Numerical Aperture	0.46	0.2	0.2
Maxium Angular Slope (°)	27	12	12

Figure 19: Optical Sensor Specs [8]

The sample to be measured was made from Schulman 1040E and formed to be a rocker panel. The part was cut to have dimensions of 25.5 by 5 cm so it would fit on the profilometer and it had a very slight amount of curvature due to the shape of the mold. The defect that was incurred during thermoforming is difficult to notice with the naked

eye, but runs down the length of the sample in the middle and looks like a valley. The sample is shown below:

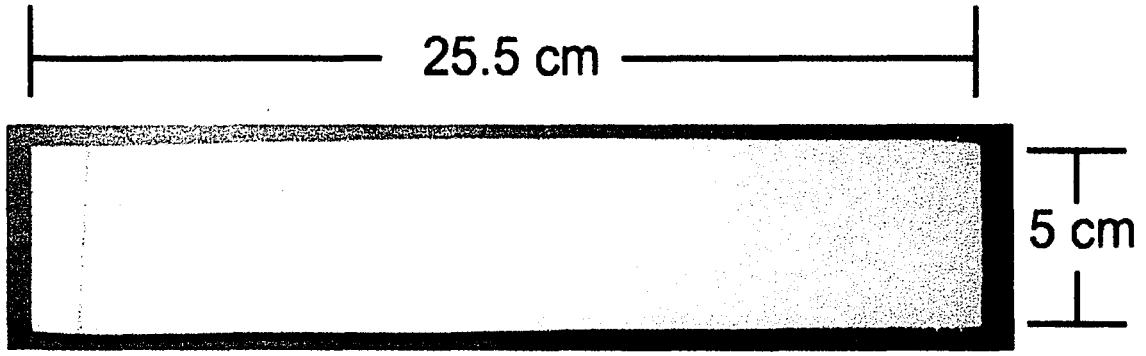

Figure 20: Schulman 1040E Sample on which Defect is Located

Although the defect was only visible on the front side, both sides of the sample were scanned in 3-D topography mode and in the line-profile mode. Optical sensor number 1 with a 10 mm measurement range, was installed first. 3-D scans of an area 35 mm long by 30 mm wide centered on the defect were performed, see Figure 21 & 22.

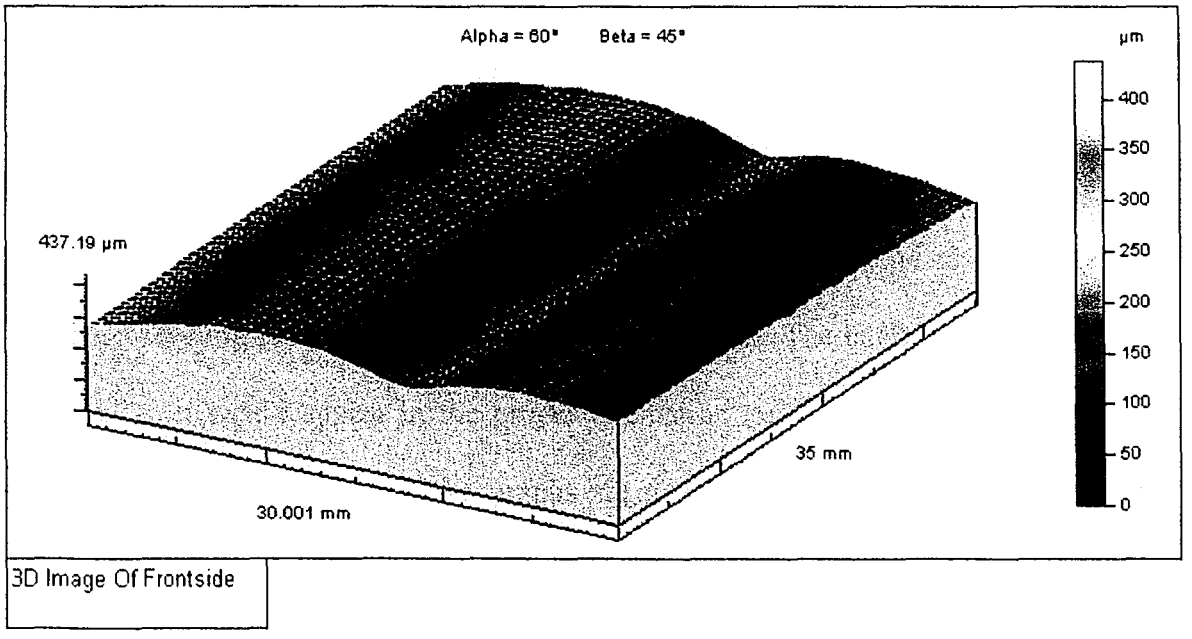

Figure 21: 3-D Image of Frontside

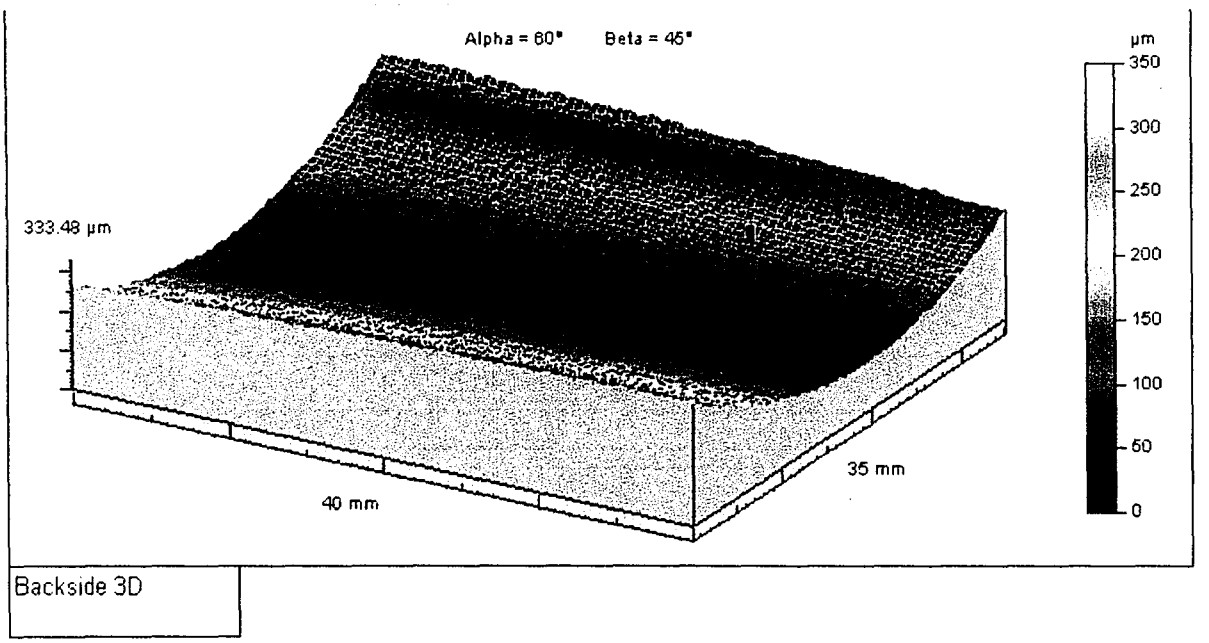

Figure 22: 3-D Image of Backside

The image scans of the front side and backside, shown in Figures 21 and 22, have clearly visible curvature, but the defect can only be seen in the scan of the front side. Next, sensor 2 with a much smaller measurement range of 350 µm and a resolution of 10 nm was setup and profile scans were taken. The profile scan holds the x axis location constant and scans over the entire width of the sample along the y axis. Scanning was performed along the same x-axis location on both the front and the backside. After manually removing any anomaly points that the sensor may have misread, the software applies a leveling feature to ensure proper data readout. The backside graph was then inverted so it would appear in the proper orientation (as if viewing the part with the defect side facing upwards). The graphs are displayed in Figures 23, the red boxes indicate the area which was later analyzed at a higher resolution.

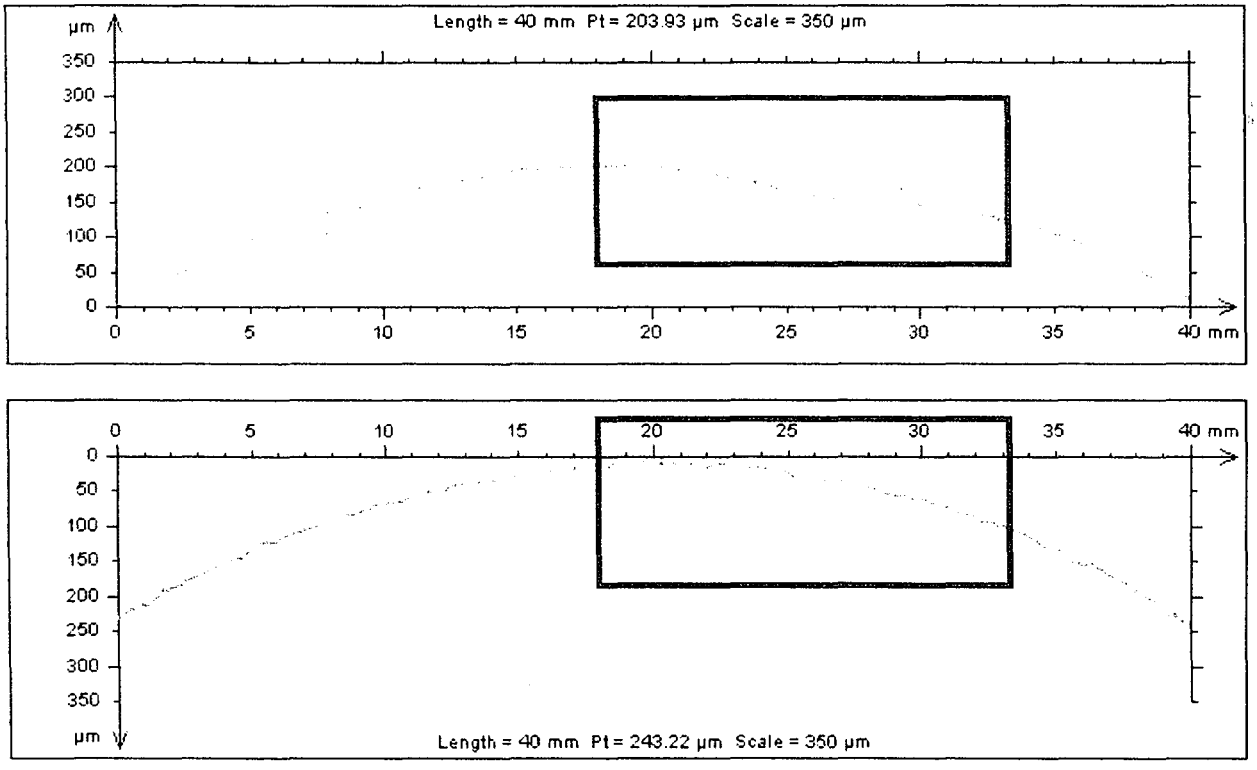

Figure 23: Profile Scans of Front and Back Sides

The defect can be seen in Figure 23 on the front side as a variation from the normal large scale curvature generated along the scan axis. Figure 24 contain scans of the area enclosed in the red boxes in Figures 23, which is the location where the defect is most prevalent.

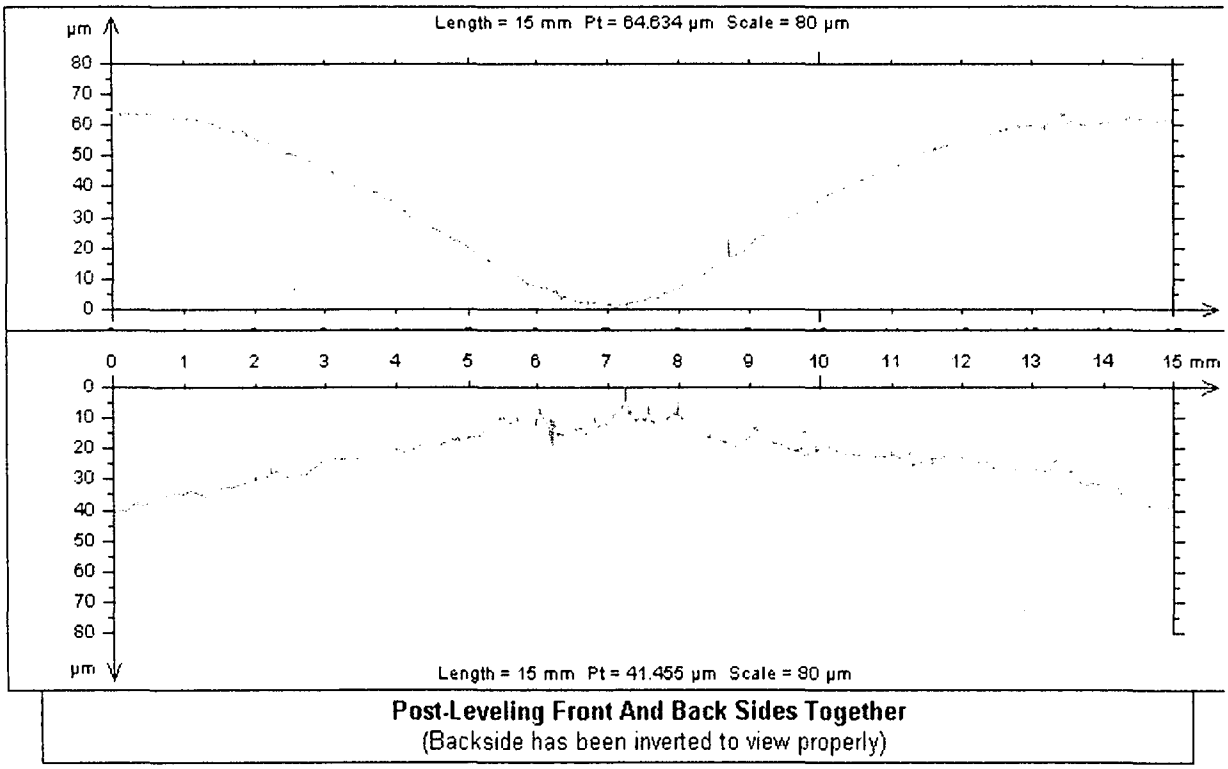

Figure 24: Zoom of Profile Scans of Front and Back Sides

In these graphs the defect shape is depicted. The front side shows a maximum difference in scanned height of 64.6 µm and the bottom surface shows a difference of 44.4 µm. Additionally, it appears that the backside has a much higher surface roughness. This side was in contact with the mold when it was thermoformed and it makes sense that it should have a higher roughness. Additionally, there was a silk-screening pattern on this side which could be contributing to the roughness detected.

After measuring the unformed thickness of a sheet as 3.3 cm, the height data of the front and back sides were imported into Excel. The data was then manipulated so that an overall thickness profile of the formed sample could be obtained. A plot of this thickness profile is shown in Figure 25.

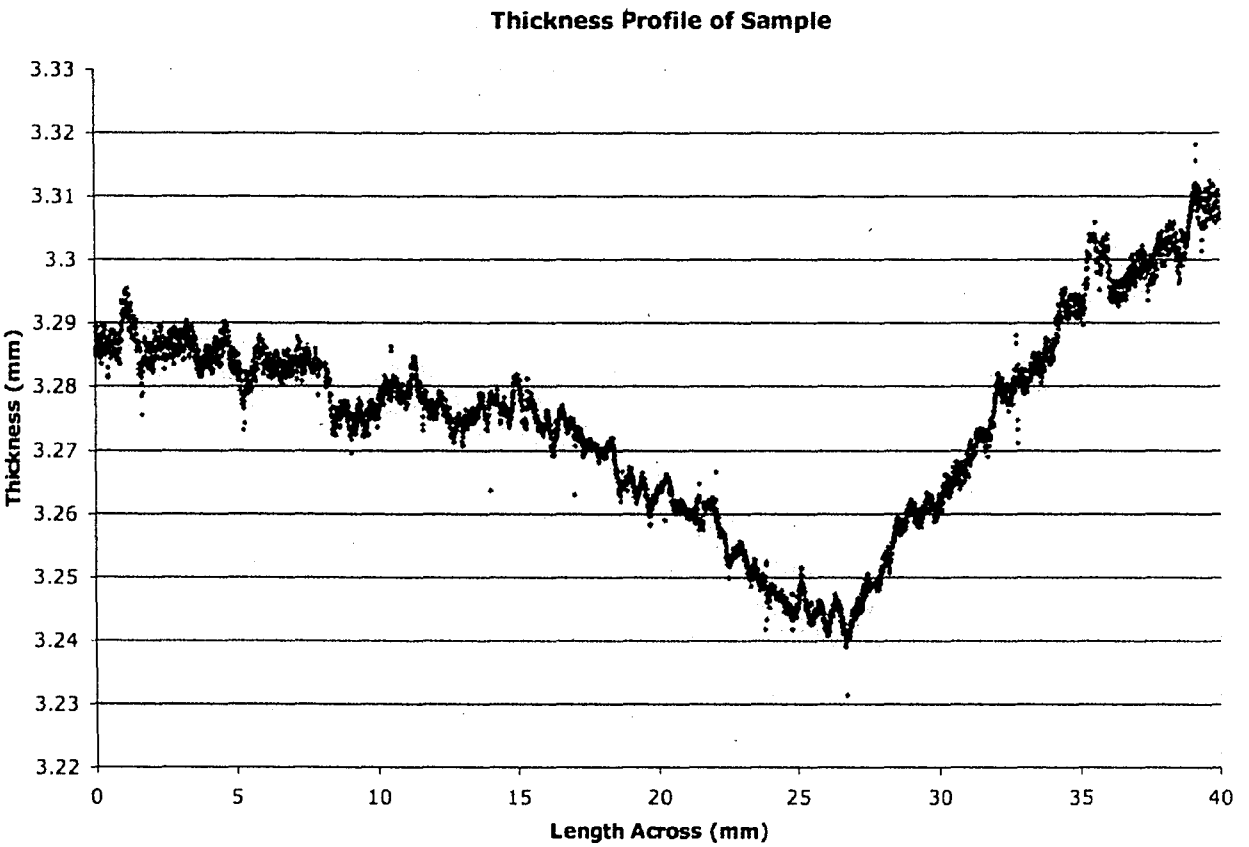

Figure 25: Thickness Profile of Sample

This data leads to the conclusion that the thinnest point on the Schulman 1040E sample is 3.23 mm thick and is located at the center of the valley. Interestingly, it shows that the area to the left of the defect is slightly thinner than the original thickness, and that the area to the right of the defect is slightly thicker. This could imply that there was a redistribution of mass from the side to the left of the defect, to the right side. Again, it should be noted that the maximum value of displacement for the valley defect is 64.6 μm.

5. Viscoelasticity

5.1 Dependent Nature

Polymers by nature are viscoelastic materials. This means that they will possess solid-like characteristics such as elasticity, strength, and structural stability and will also exhibit liquid like characteristics such as flow, all which depend on time, temperature, loading rate and loading amount.

> In viscoelastic materials when a stress is applied to the body, the strain state depends on the manner in which the stress is applied, i.e. whether the load is applied rapidly or slowly. Thus the history of loading must be considered as well as the magnitude of the load. In addition, a viscoelastic body will not maintain a constant deformation under a constant stress, regardless of the loading pattern, rather it will deform or creep with increasing time. Also, if such a body is constrained at constant deformation, the stress required to hold it gradually diminished, or relaxes. [3]

This is the result of the polymer chains' ability to uncoil as a load is applied due to disentangling and slippage of the chains over chains.

For viscoelastic materials the result of a strain input test is a time dependent ratio of stress to strain which is called the stress relaxation modulus. The shear relaxation modulus is designated $G^*(t)$, the bulk relaxation modulus is $K^*(t)$, and the tensile modulus is $E^*(t)$. It is customary to display these properties on log plots and all figures will be displayed this way. Since viscoelastic materials behave like a combination of a solids and a liquid it is useful to define these moduli in complex terms, which is a measure of the material's resistance to deformation. By performing dynamic testing the stress can be transformed into to parts: An elastic stress (σ' or τ') which is in phase with the strain, and a viscous stress (σ'' or τ'') which is 90° out of phase with the strain. With

this data the elastic modulus, or storage modulus (E' or G') and the viscous modulus, or loss modulus (E'' or G'') can be calculated directly. [3,5,9]

$$E^*=\sigma^*/\varepsilon \qquad G^*=\tau^*/\gamma$$
$$E^*=E'+iE'' \qquad G^*=G'+iG'' \tag{8}$$

Storage Moduli:

$$E'=\sigma'/\varepsilon \qquad G'=\tau'/\gamma \tag{9}$$
$$E'=E^*\cos(\delta) \qquad G'=G^*\cos(\delta)$$

Loss Moduli:

$$E''=\sigma''/\varepsilon \qquad G''=\tau''/\gamma$$
$$E''=E^*\sin(\delta) \qquad G''=G^*\sin(\delta) \tag{10}$$

Where δ is the phase angle, σ is the tensile stress, τ is the shear stress, ε is the tensile strain, γ is the shear strain. [5]

Additionally it should be noted that E is related to G by:

$$E = 2\cdot(1+\nu)\cdot G \tag{11}$$

Where ν is Poissons ratio and is usually assumed to be 0.5 (perfectly incompressible).

5.2. Glass Transition Temperature and Melt Temperature

The plastics are most thermoformable when their temperature is above the glass transition temperature, T_G, for amorphous polymers and near the melt temperature, T_M, for crystalline polymers. Generally, there is no single temperature when the plastic is

ready to be formed, but rather there is a range of temperatures when the material becomes soft enough to form. Typically, this range is usually 30-70 °C above T_G for amorphous polymers. For crystalline polymers this range is usually within a few degrees above or below T_M. [1,2] As the temperature of a polymer climbs above T_G, its ductility increases and can yield at very low strain levels. Figure 26 illustrates the temperature dependence of stress and strain for an amorphous polymer. It can be seen that as the temperature increases the polymer is able to endure significantly more strain before failure.

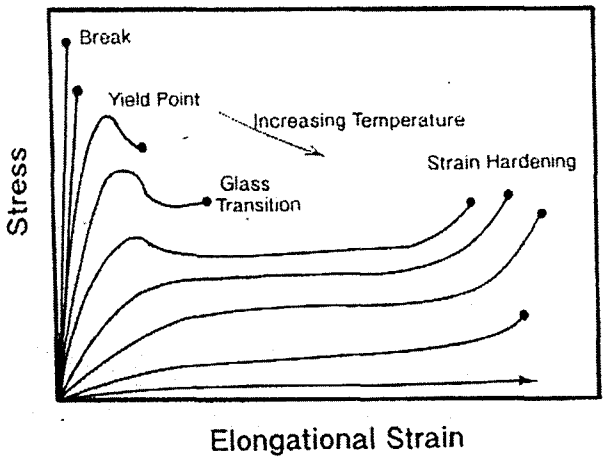

Figure 26: Stress vs Strain as Related to Increasing Temperature [1]

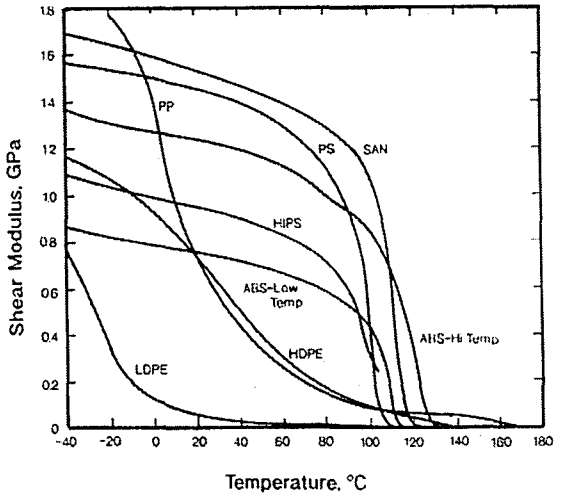

Figure 27: Shear Modulus vs Temperature for Various Polymers [1]

Mechanically this occurs in the polymer because the shear modulus is dependant on temperature as seen in Figure 27. As temperature increases, shear modulus decreases in a non-linear fashion. This effect is show in the graph above for many polymers. The sharp drop in shear modulus corresponds with the material's glass transition temperature.

At the higher temperatures and above of the forming ranges the thermoplastics may begin to discolor, bubble, smoke, or sag excessively. During the heating phase sheet sag will occur since the force of gravity is enough to deform a sheet suspended in air or clamped.

The sheet is ready to be formed when temperature at all points within the sheet are in the forming range. Graphs for thick and thin gauge sheets showing when the forming range has been reached as a function of time are show in Figures 28 and 29.

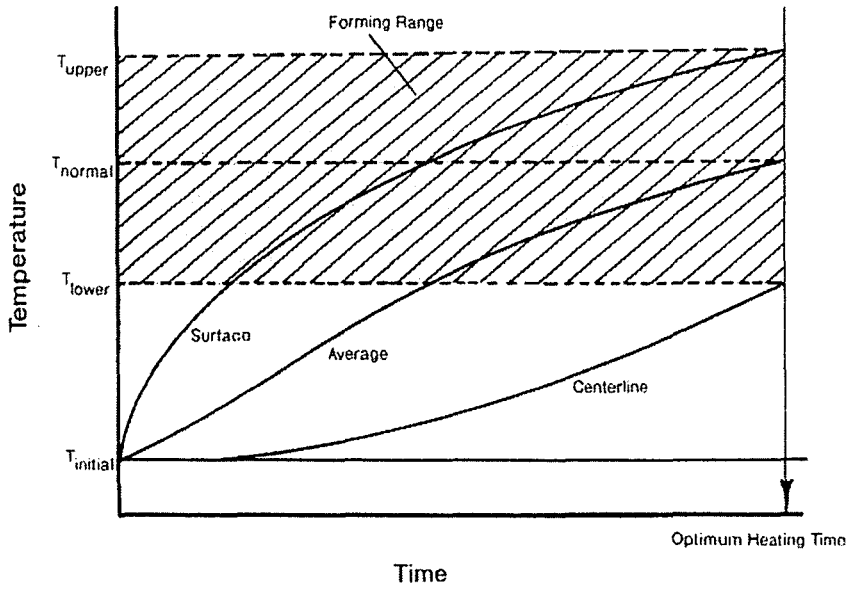

Figure 28: Forming Temperature Range for Thick Sheets [1]

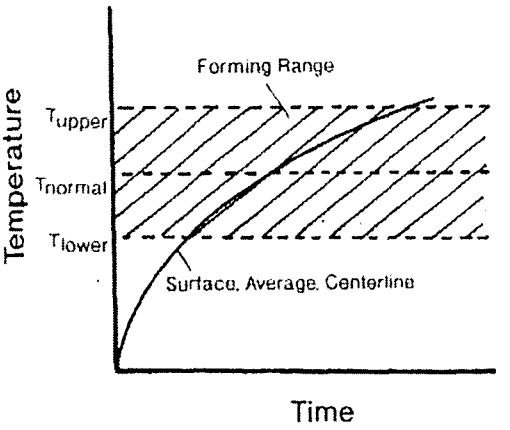

Figure 29: Forming Range for Thin Sheets [1]

Air temperature can be monitored with the use of thermocouples and sheet surface temperature can be determined with the use of infrared devices such as pyrometers and cameras. Computers can analyze the data and detect if top and bottom surface temperatures are in the forming range and make split second decisions as to when the sheet is ready to be formed.

6. Thermal Properties of Polymer Sheets

The thermal properties of the polymers will play a large role in the way the polymer behaves during thermoforming. A table showing values for a variety of polymers at 25°C is shown in Figure 30. The heat capacity, at a constant pressure, is a defined as the isobaric change in polymer enthalpy with temperature. (12)

$$c_p = \left(\frac{\partial H}{\partial T}\right)_p$$

This value is the slope of the enthalpic curve and is only slightly dependent on temperature for amorphous polymers, but can vary greatly above T_M for crystalline

polymers. The temperature dependent heat capacity curve can be obtained by performing a Differential Scanning Calorimetry (DSC) test.

The thermal conductivity, k, of polymers occurs through molecular interaction as opposed to electron transfer as in metals. Though it is difficult to measure, it is not very temperature dependent, so a value obtained at any temperature can be used.

Thermal diffusivity of the polymer is the rate at which energy is transferred and can be calculated using the above-mentioned properties and the material's density. Using the equation below:

$$\alpha = \frac{k}{\rho c_p} \tag{13}$$

Thermal expansion occurs as polymeric materials are heated and can be experimentally measured by performing a Thermal Mechanical Analysis (TMA) test on a sample. These values can be significant enough to have an effect on the overall final part shape after cooling, and this effect must be taken into consideration during mold design. It can also cause wrinkling during the heating phase. Since the polymer sheet is clamped as the material expands the volume begins to overflow from the defined clamp area and the sheet will form small buckles or wrinkles. As heating continues to occur these wrinkles can relax out of the sheet as it continues to sag due to the decreasing relaxation modulus as time increases. However, if the wrinkles are big enough they can cause a defect in the part, which will then be noticeable after forming.

Polymer	Density	Thermal Conductivity	Heat Capacity	Thermal Diffusivity	Thermal Expansion Coefficient
	kg/m^3	$(cal/s\ cm\ ^\circ C)x10^{-4}$	$(cal/g\ ^\circ C)$	$(cm^2/s)x10^{-4}$	$(^\circ C^{-1})x10^{-6}$
Polystyrene	1050	4.3	0.54	7.66	70
PMMA	1200	4.3	0.615	5.9	70
ABS	1050	2-3	0.4	4.8-7.1	60-130
Polycarbonate	1200	5	0.49	8.5	60-70
Rigid PVC	1350	3.45-4.1	0.365	7-8.4	70-80
LDPE	920	7.57-9.6	0.88-1.05	7.85-11.9	250
HDPE	960	9-12.1	0.88-1.15	8.1-14.3	200
Cellulose Acetate	1300	5.2	0.67	5.9	120
Polypropylene	900	4.1-4.2	0.83	5.5-6.92	150

Figure 30: Thermal Properties of Thermoformable Polymers at 25°C [1]

7. Observation of Sag Behavior

When a clamped thermoplastic sheet is heated it will begin to sag above a certain temperature. The maximum tensile strain is located on the bottom surface and the maximum compressive strain is on the top surface. For a rectangular sheet sag can be calculated by [1]:

$$y = \frac{-\beta q L^4}{E(T)h^3} \tag{14}$$

Where y is the sag amount in inches, q is the weight of the sheet in lb/in^2, L is the sheet span in inches, E(T) is the temperature dependent modulus in lbF/in^2, β is a function of sheet length to width shown in Figure 31.

(Sheet length)/(sheet width)	β
1.0	0.0444
1.2	0.0616
1.4	0.0770
1.6	0.0906
1.8	0.1017
2.0	0.1110
3.0	0.1335
4.0	0.1400
5.0	0.1417
infinity	0.1421

Figure 31: Scale Factor for Equation 14 [1]

8. TPO Property Characterization

Ford had two types of Thermoplastic Olefin polymer sheets they wished to have characterized. The first polymer was Hifax TBC 756T, a compounded polyolefin manufactured by Basell. This impact modified polypropylene homopolymer is 25% talc-filled and has a density of 1.06 g/cm^3. [12] The second polymer is Polytrope TPP 1040E, manufactured by A. Schulman, and is an olefinic elastomer with a density of 1.08 g/cm^3. [13] Little information other than this was provided by the manufactures as these polymers are proprietary blends, thus further tests were performed in Lehigh's Materials Science laboratories to quantify the differences between these two polymers.

8.1. Dynamic Mechanical Analysis Measurements of Samples

Tests were performed on TA Instruments' DMA 2980 Dynamic Mechanical Analyzer. The machine, fitted for a 3-point bending clamp, applies a deformation to the sample via a drive motor by sinusoidally loading the sample at an oscillatory amplitude of 15μm. At the same time, the clamping system is in a controlled oven, which provided a stepwise temperature pattern. The temperature was swept from 35°C to 170°C in 5°C

increments and was then held constant at each level for 5 minutes. At temperatures higher than 170°C, the polymers become too soft and the test data would no longer have been valid. The load oscillation frequency was also applied in a stepwise manner at each temperature level. Frequencies included 20, 10, 5, 1, 0.5, 0.1 and 0.05 Hz. The samples inserted into the clamp system had a length of 50 mm, width of 12.71, (cut to fit in machine) and thickness of 3.02 mm (normal sheet thickness).

The DMA machine measures the raw signals of force, amplitude of deformation, and phase angle. Internal constants from calibrations are applied and from this data the sample's complex stiffness (K′ and K″) are calculated. Once this stiffness is obtained, the software outputs the Elastic Modulus, E, based on the following equation:

$$E = K_s \cdot \frac{L^3}{6I}\left[1 + 12/5 \cdot (1+\nu) \cdot \left(\frac{t}{L}\right)^2\right] \qquad (15)$$

Where:

E = Elastic Modulus
L = Sample Length
t = Sample Thickness
I = Sample Moment of Inertia
ν = Poison's Ratio
Ks = Measured Stiffness (Force applied to the sample divided by the amplitude of deformation)

Test data for the Basell and Schulman Materials were then analyzed in Excel and results for the Storage and Loss Elastic Moduli (E′ and E′) of both materials are displayed in Figures 31 and 32. Both E′ and E″ are higher in the Schulman 1040E than in the Basell 756T for all temperatures tested. The temperature reproducibility is +/- 2°C and the modulus precision is +/- 1%. [5]

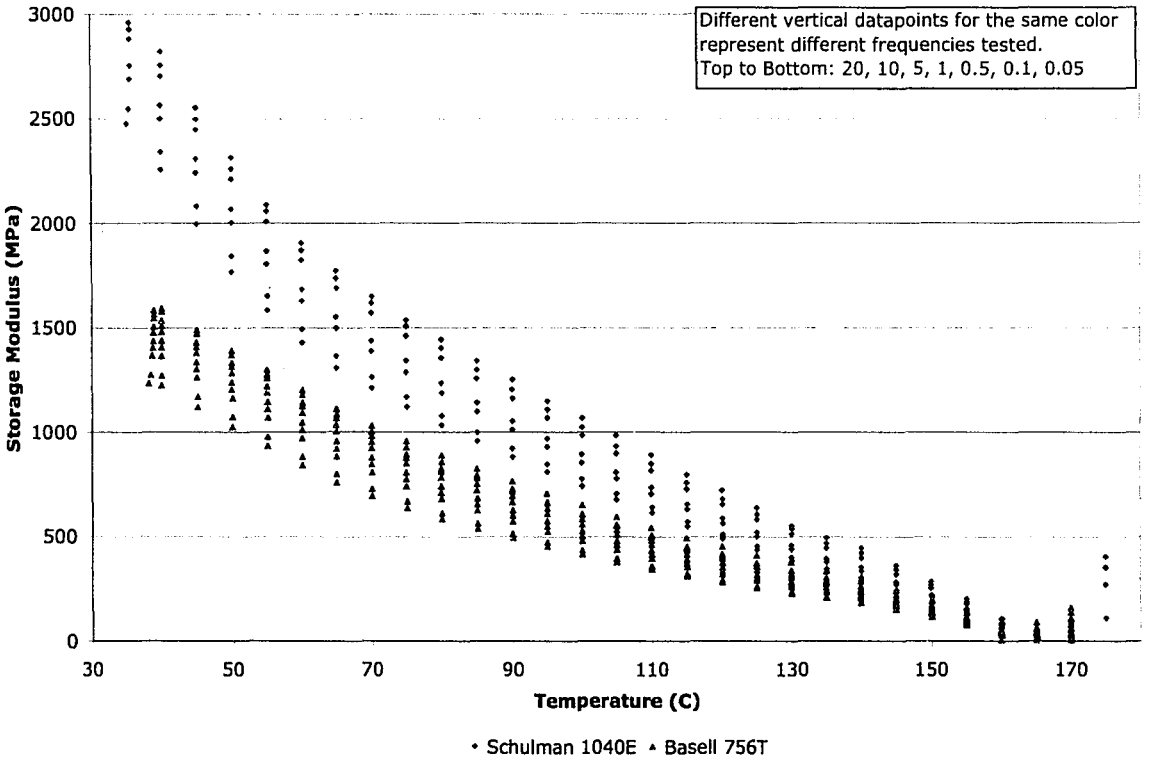

Figure 32: Storage Modulus (E′) vs Temperature – Basell 756T and Schulman 1040E

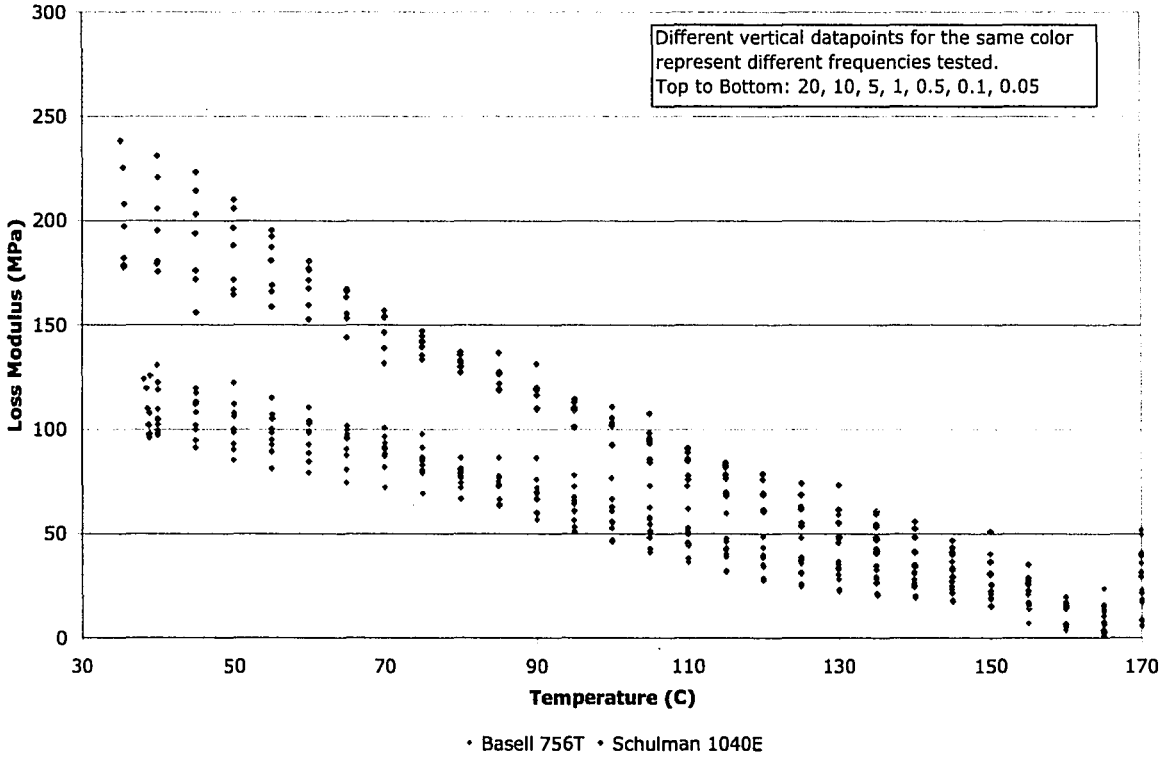

Figure 33: Loss Modulus (E″) vs Temperature – Basell 756T and Schulman 1040E

8.2. Differential Scanning Calorimetry Measurements of Samples

The samples were then tested in TA Instrument's DSC 2920 differential scanning calorimeter. "If a sample and an inert reference are heated at a known rate in a controlled environment, the increase in sample and reference temperature will be about the same (depending on specific heat differences), unless a heat-related change takes place in the sample. If this change takes place, the sample temperature either evolves or absorbs heat. In DSC, the temperature difference between sample and reference from such a heat change is directly related to the differential heat flow." [4] The setup and operation of the machine is described as follows:

> The standard DSC cell uses a constantan (thermoelectric) disc as a primary heat-transfer element. A silver heating block, capped with a vented silver lid encloses the constantan disc. The selected sample and an inert reference are placed in pans that sit on raised portions of the disc. Heat is transferred through the constantan disc to both the sample and the reference pans. Differential heat flow to the sample and reference are monitored by the chromel-constantan area thermocouples. The thermocouples are formed at the junctions of the constantan disc and the chromel wafers welded to the underside o the two raised portions of the disc. Chromel and alumel wires are connected to the chromel wafers at the thermocouple junctions to measure sample temperature. The alumel wire welded to the reference wafer is for the thermal balance.
>
> Pure gas, entering the heating block through an inlet in the DSC cell's base plate, is preheated to block temperature by circulation before entering the sample chamber through the pure gas inlet. Gas exits through the bent hole in the silver lid.
>
> Vacuum and air cooling ports on the DS 2920 lead to openings in the cell but not directly to the sample chamber. A bell jar, placed over the cell and sealed with an O-ring, protects the operator from evolved gases and permits cell evacuation. [4]

Semi-crystalline polymers have very distinctive properties noticeable during heating. Upon reaching the onset of the melt temperature, T_M, the heat flow makes a characteristic

spike. This spike is used by the software to determine melt onset temperature, peak melt temperature, and the heat of fusion.

Samples of the Basell 756T and Schulman 1040E polymers were prepared in the reference pans and inserted into the DSC. The test method was then loaded on the computer, which consisted of equilibrating at 25°C and then ramping up the temperature at 10°C/min to 225°C. The test was conducted 3 times with each sample to ensure repeatability with the data shown in Figure 34:

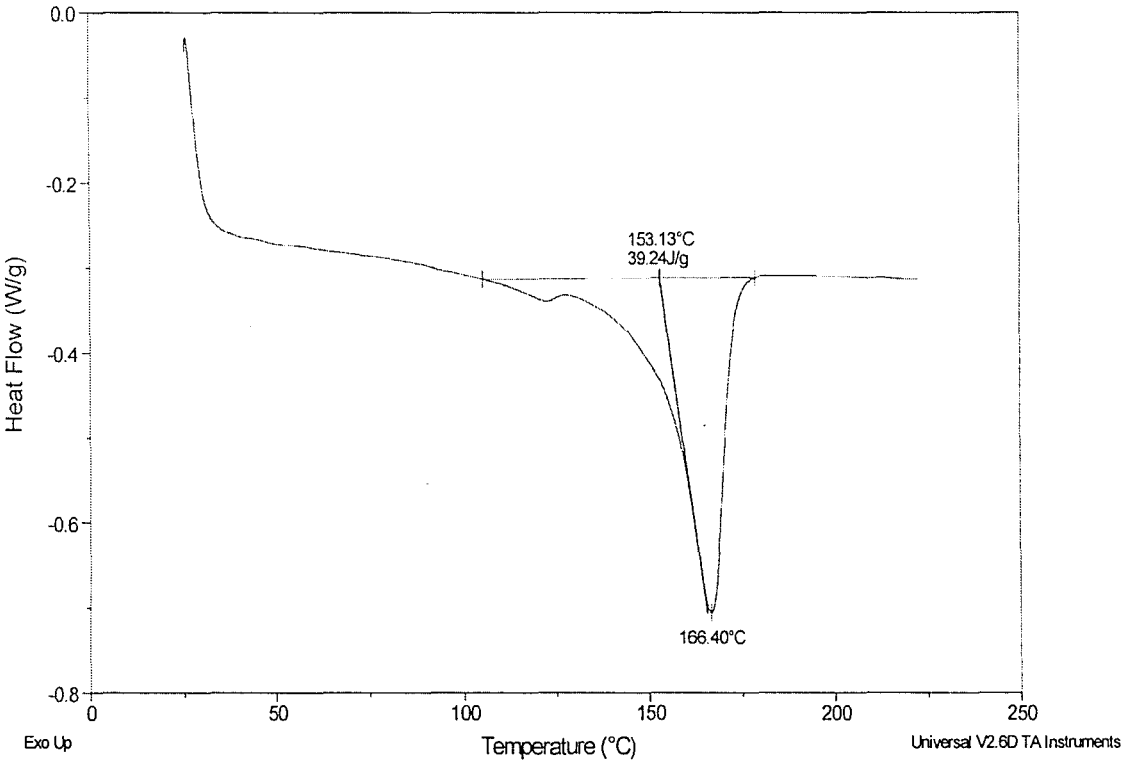

Figure 34: Results from DSC test for the Basell 756T

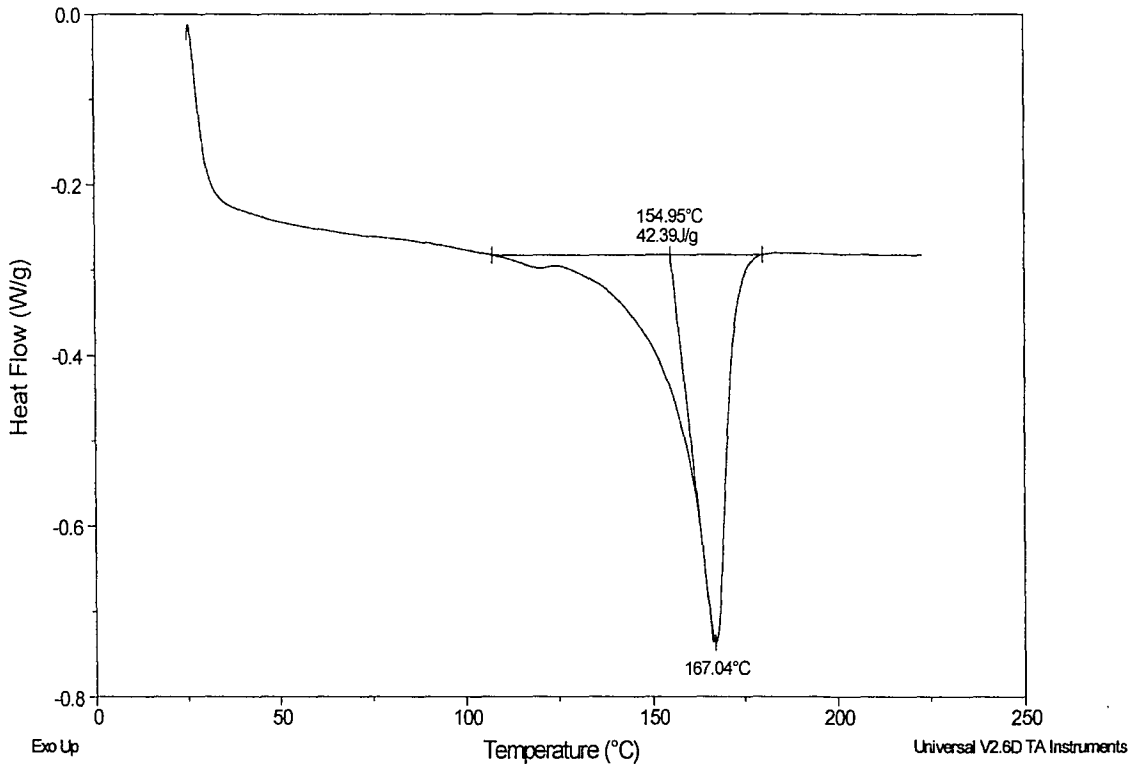

Figure 35: Results from DSC test for the Schulman 1040E

These results indicate that the Basell 756T has a Melt Onset Temperature of 153.1°C a Peak Melt Temperature of 166.4°C and a Heat of Fusion of 39.24 J/g. Likewise, the Schulman 1040E has a Melt Onset Temperature of 154.95°C a Peak Melt Temperature of 167.04°C and a Heat of Fusion of 42.39 J/g.

9. Viscoelastic Behavior and Time Temperature Superposition

Parts thermoformed at Ford's R&D lab had a typical forming range of 160°C to 190°C. [6] As previously mentioned, when heating the sheets in the temperatures below the forming range they experienced buckling and warping. Thus, 130°C was chosen as the reference temperature for construction of a Stress Relaxation Master Curve. This master curve can be adjusted using shift factors to display the stress relaxation at other

temperatures. The principle behind time temperature superposition is that there exists a relationship between time-scale and temperature to describe the viscoelastic behavior of a polymer. "That is, the general behavior of a material at two different temperatures is qualitatively the same except that it requires a loner time to exhibit its response at one temperature than another."[3] A master relaxation curve at a reference temperature, is constructed by manipulating the storage modulus data found using the DMA machine. First, the data is sorted by ascending temperature and then inside each temperature range by ascending frequency. A reference temperature is selected, e.g. 130°C, and the modulus is graphed versus the set of frequencies tested at on a log-log scale. The next temperature set is then analyzed. The group of frequencies for that temperature are multiplied by a shift factor, a_t, until the modulus aligns alongside the previous data set. This process is continued for all temperatures until a smooth curve is obtained. Figures 36 and 37 are the result of this process when performed on the Basell 756T and Schulman 1040E data sets. In Figure 36, the two most left data sets were considered anomalies and not used in further calculations since they did not align properly for any amount of shift factor used.

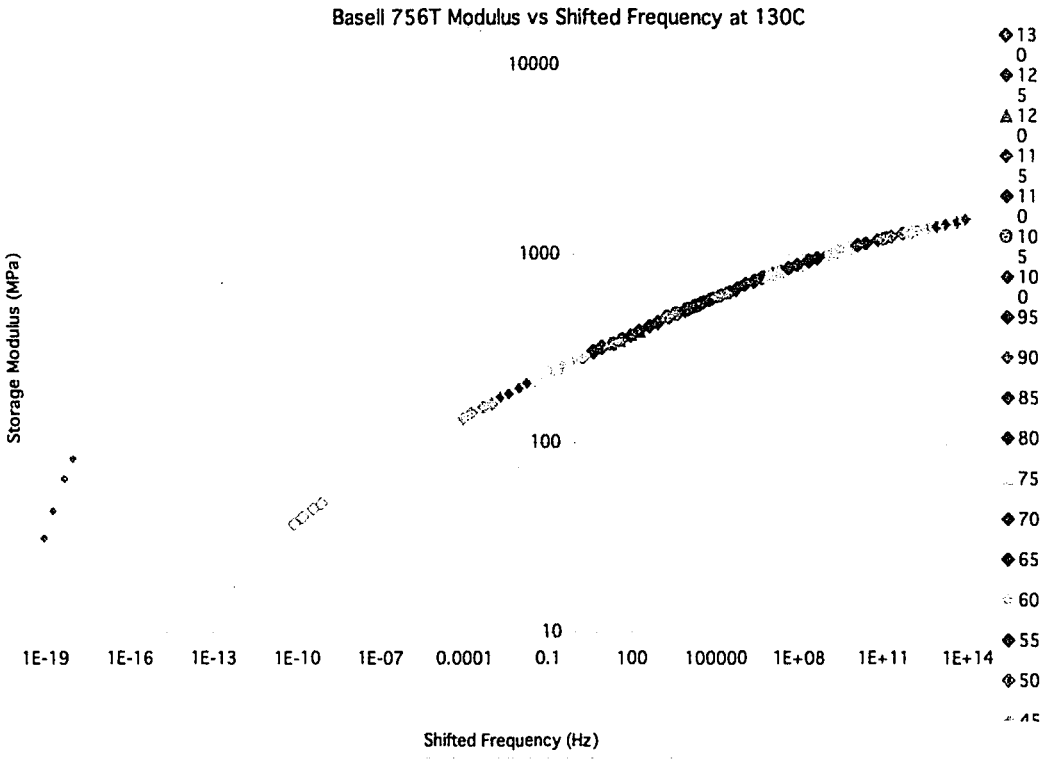

Figure 36: Basell 756T Modulus vs Frequency at 130°C
Note - the two most left data sets were considered anomalies and not used

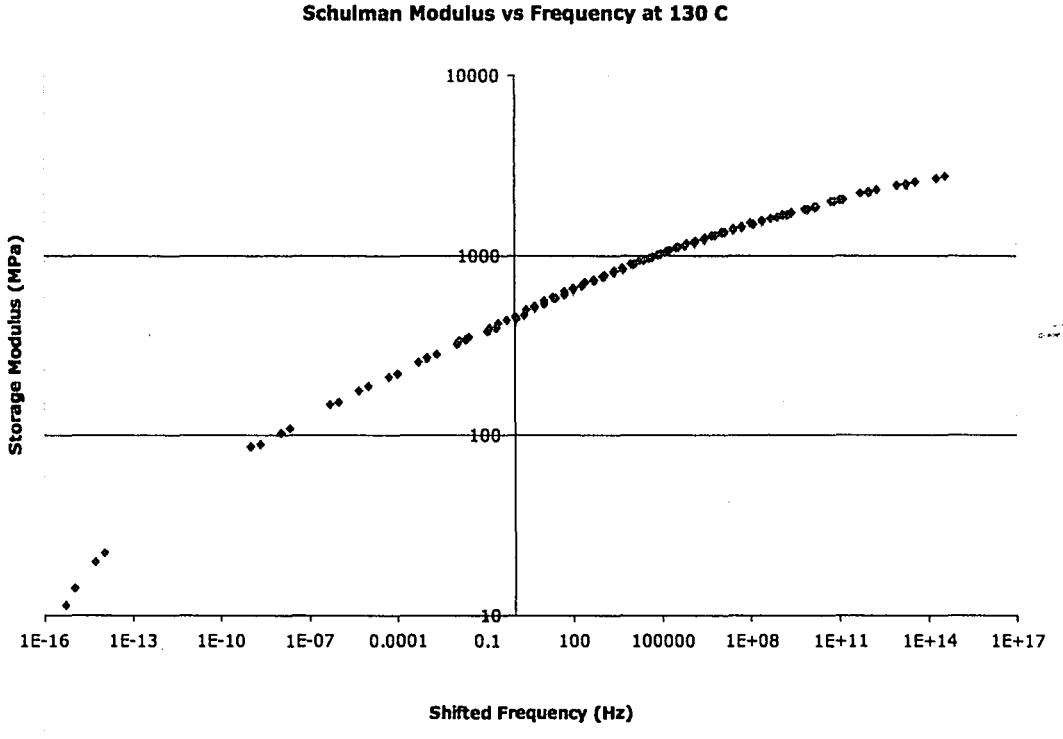

Figure 37: Schulman 1040E Modulus vs Frequency at 130°C

Now that smooth graphs of the storage modulus versus the shifted frequency have been created, a master relaxation curve can be constructed. A new data set of calculated time is created by taking the inverse of the shifted frequencies. The modulus can be graphed versus the calculated time. The result is a curve describing the stress relaxation behavior of the polymer at a specific temperature as a function of time. Results for the Basell 756T and Schulman 1040E are displayed in Figure 38 over 25 decades of time at 130°C.

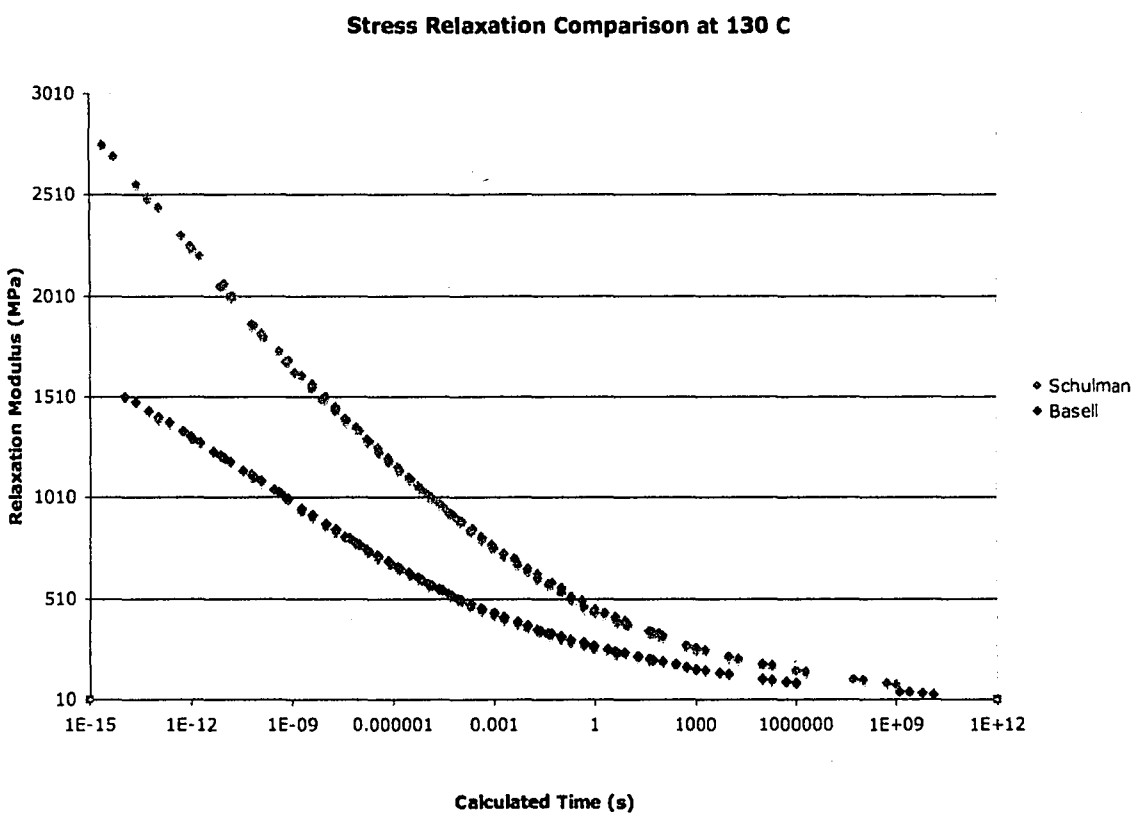

Figure 38: Stress Relaxation: Basell 756T vs Schulman 1040E – only x-axis in log scale

As expected, the two materials are seen to exhibit similar stress relaxation behavior, since they are both TPO polymer blends. However, it should be noted that the relaxation modulus of the Schulman 1040E is consistently higher.

Figure 39 is a section of what the Excel spreadsheet used to obtain the graph in Figure 38 looks like:

Time (min)	Temperature (C)	Storage Modulus (MPa)	Frequency (Hz)	Shift Factor a_t	Shifted Frequency	Calculated Time (s)	Temp (K)	1/T (1/K)
18.2217	40	2500.46	0.5	4.00E+13	2E+13	5E-14	313	0.003194888
17.0763	40	2563.99	1	4.00E+13	4E+13	2.5E-14	313	0.003194888
16.886	40	2704.01	5	4.00E+13	2E+14	5E-15	313	0.003194888
16.7342	40	2755.14	10	4.00E+13	4E+14	2.5E-15	313	0.003194888

Figure 39: Excel Sheet Sample

Graphs of the shift factors for the two polymers can be seen in Figure 40 and 41:

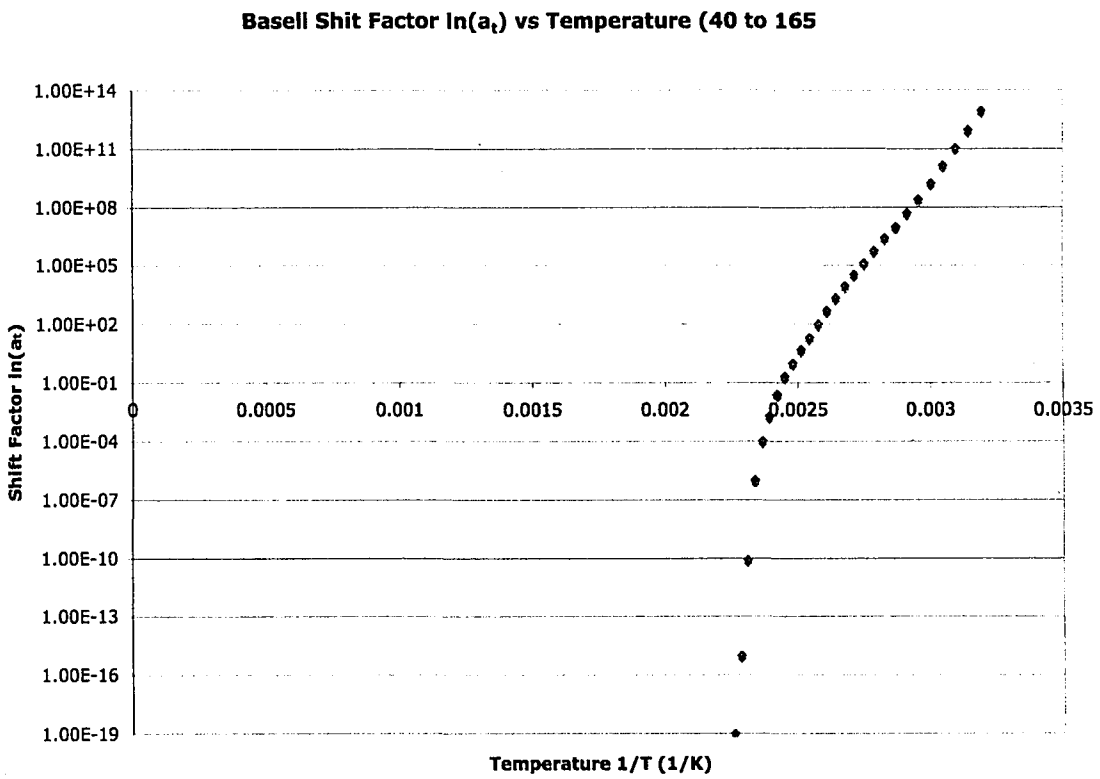

Figure 40: Basell 756T Shift Factors

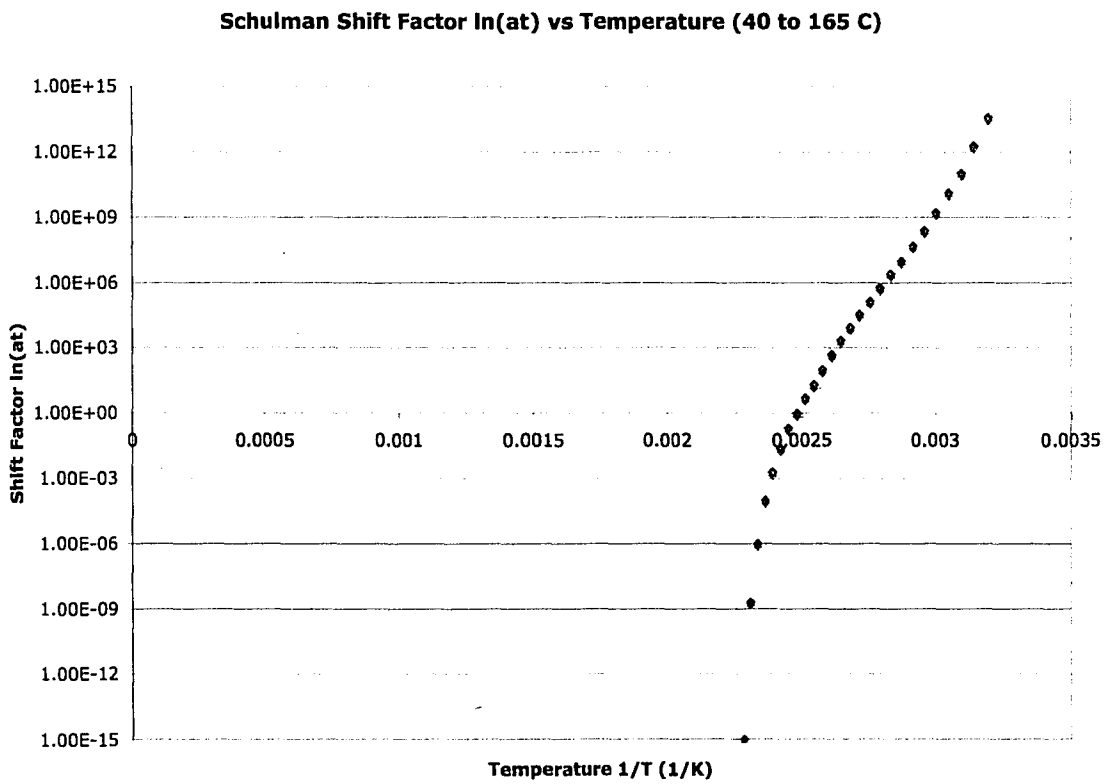

Figure 41: Schulman 1040E Shift Factors

10. Prony Series Data Curve Fits

The relaxation modulus data needed to be fit to a curve to be usable by the FEM simulation software, ANSYS. However, ANSYS only accepts the shear relaxation modulus G′ as an input parameter so equation (11) was used to convert the tensile relaxation modulus E′ to the shear relaxation modulus G′. ANSYS has a prony series curve fit generator built in and this was used to generate the prony series. "The initial values you choose for your coefficients will determine the success of your viscoelastic curve fitting operations." [10] To obtain best results, decade values, labeled st_N (N ranges from 1 to 10), should be equally distributed in the log scale, so that they span the

entire data range and are input as fixed values. Thus coefficient values were input according to Figure 42.

Coefficient Index	Coefficient Name	Basell 756T Coefficient Value	Schulman 1040E Coefficient Value	Fixed ?
1	sa_0^2	1	1	N
2	sa_1^2	1	1	N
3	st_1	1.00E-14	1.00E-14	Y
4	sa_2^2	1	1	N
5	st_2	1.00E-11	1.00E-11	Y
6	sa_3^2	1	1	N
7	st_3	1.00E-08	1.00E-08	Y
8	sa_4^2	1.000	1.000	N
9	st_4	1.00E-05	1.00E-05	Y
10	sa_5^2	1	1	N
11	st_5	0.01	0.01	Y
12	sa_6^2	1	1	N
13	st_6	1	1	Y
14	sa_7^2	1	1	N
15	st_7	100	100	Y
16	sa_8^2	1	1	N
17	st_8	10000	10000	Y
18	sa_9^2	1	1	N
19	st_9	1.00E+06	1.00E+06	Y
20	sa_10^2	1	1	N
21	st_10	1.00E+08	1.00E+08	Y

Figure 42: Initial Inputs for 10-Term Prony Series Fit

ANSYS then compares the curve created by the input coefficient values to the G′ values and adjusts the coefficients that are not fixed so the best prony series fit results. The adjusted coefficients for the Basell 756 and Schulman 1040E can be seen in Figure 43.

Coefficient Index	Coefficient Name	Basell 756T Coefficient Value	Schulman 1040E Coefficient Value
1	sa_0^2	3.747	5.263
2	sa_1^2	12.183	12.575
3	st_1	1.00E-14	1.00E-14
4	sa_2^2	10.29	14.475
5	st_2	1.00E-11	1.00E-11
6	sa_3^2	10.334	12.819
7	st_3	1.00E-08	1.00E-08
8	sa_4^2	9.382	12.106
9	st_4	1.00E-05	1.00E-05
10	sa_5^2	7.127	9.808
11	st_5	0.01	0.01
12	sa_6^2	5.270	5.141
13	st_6	1	1
14	sa_7^2	4.960	6.168
15	st_7	100	100
16	sa_8^2	4.349	6.441
17	st_8	10000	10000
18	sa_9^2	3.327	5.109
19	st_9	1.00E+06	1.00E+06
20	sa_10^2	3.581	5.141
21	st_10	1.00E+08	1.00E+08

Figure 43: Prony Series Coefficients Calculated by ANSYS

The "ANSYS Curve Fitted Equation" can be seen in equation (16). [10]

$$G' = (sa\_0)\text{^}2 + \sum_{i=1-N}^{N} (sa\_i)^2 \cdot e^{-(st\_i)*t} \tag{16}$$

The resulting curve fits can be seen below compared to the actual data in Figures 44 and 45.

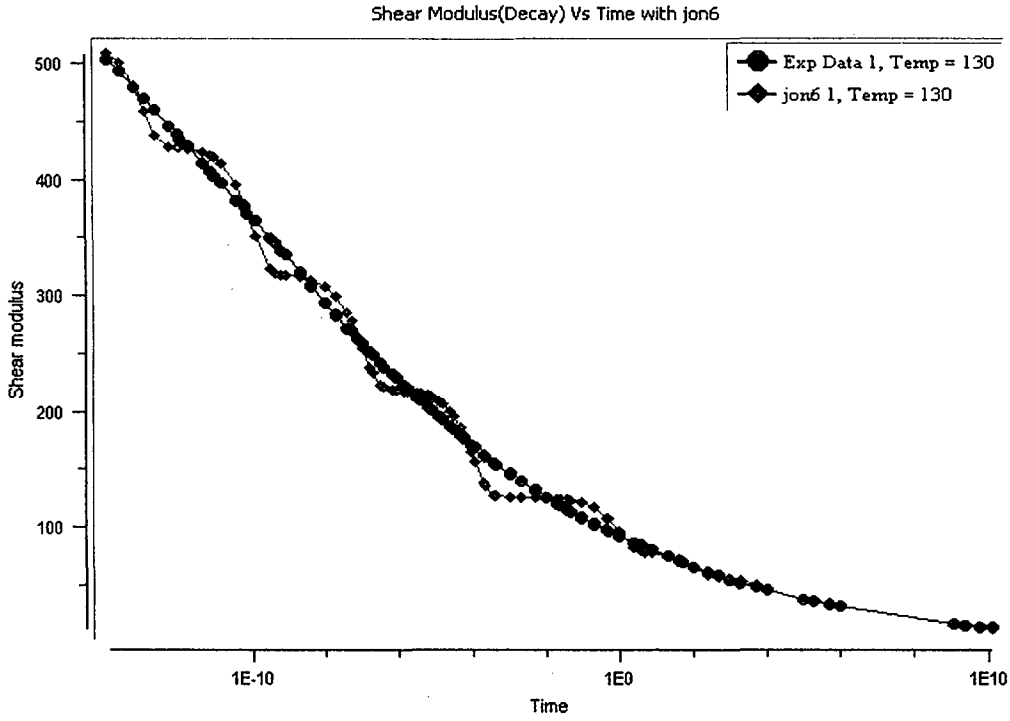

Figure 44: 10-Term Prony Series Curve Fit For Basell 756T G′ Data

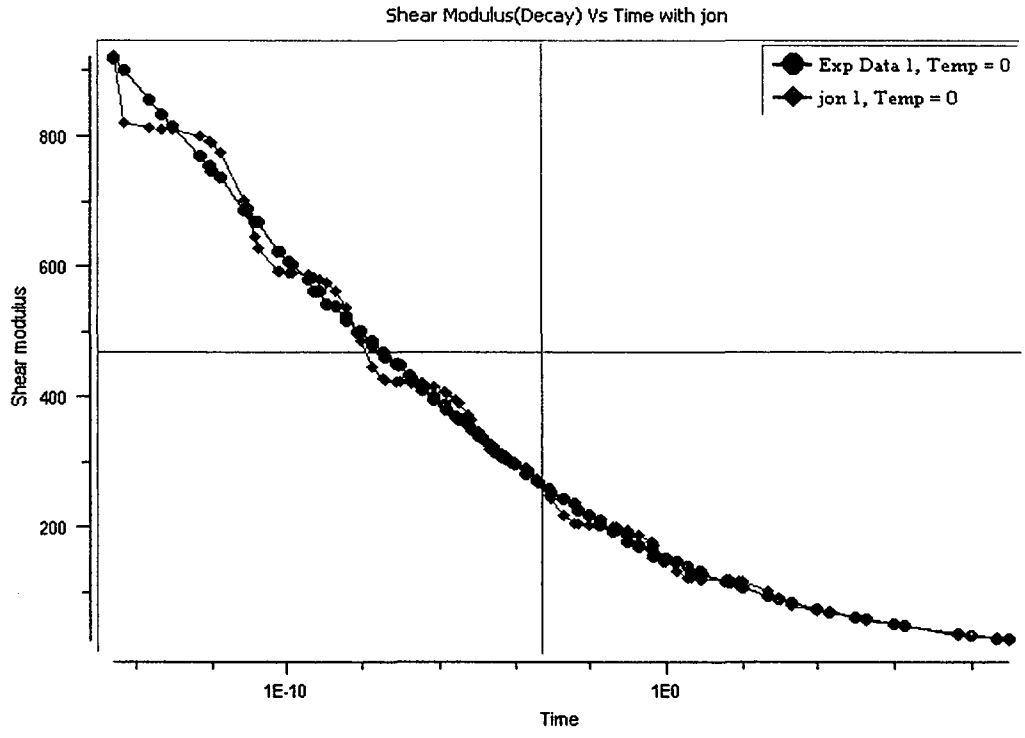

Figure 45: 10-Term Prony Series Curve Fit For Schulman 1040E G′ Data

11. ANSYS Simulation of Defect Formation Mechanisms

With the defect now quantifiably measured, the viscoelastic relaxation data and other known material properties were input into ANSYS engineering analysis software to attempt to replicate defect formation. A simulation was performed to simulate the sagging behavior of the Basell 756T polymer sheets at 130°C to see if the rippling observed during actual sheet heating could be replicated as a result of sag and subsequent contact with the mold surface. A 2-D simulation was programmed where a beam of thickness 3mm and 200 mm long, created using membrane elements, was loaded with the force of gravity at 130°C. The material properties used were the prony series data seen in Figures 43 and 44. A 2-D model was chosen because it can accurately represent a long channel being formed (similar the the geometry of the door claddings) due to the plane strain conditions.

The beam created was loaded with gravity at 130°C for 60 seconds, simulating a sheet sitting in the oven at 130°C for one minute. The sheet sagged downward as expected, however, no rippling was observed. This indicates that the ANSYS model does not contain sufficient detail to properly simulate the physics of defect formation on the micro-scale. The model is certainly an oversimplified version of the actual processes that are at work. Air entrapment, surface roughness, temperature gradients within the sheet, material inhomogeneity, or other factors could be at work at the same time creating the observed defect.

Another simulation was performed using a hyper-elastic model for polymer material properties where a flat plate was brought into contact with a sagging polymer

sheet that started with a defect in it. This would simulate what might occur if a "wave," as seen in the heating of TPO polymer sheets at Ford R&D, were to remain trapped in the sheet as the mold came into contact with it. [6] The sequence of pictures seen in Figures 46-48 show the progression of the simulation.

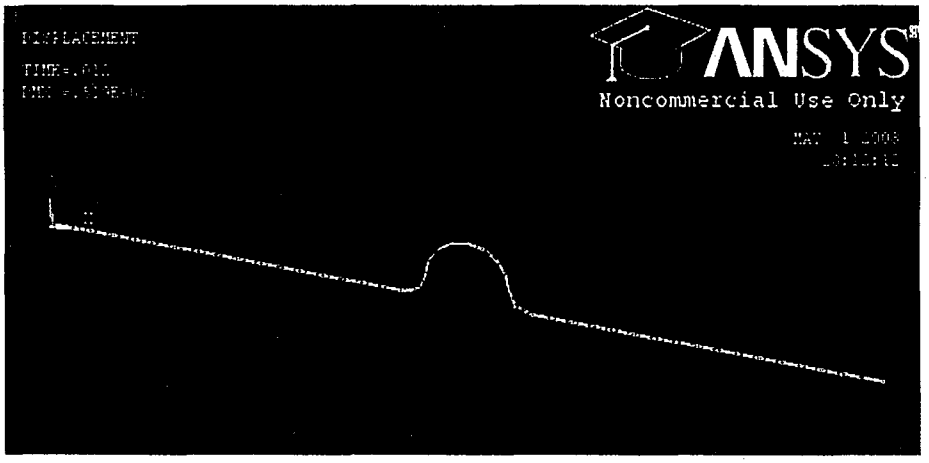

Figure 46: ANSYS Simulation: "Wave" Defect Initially in Sheet, Time = .012 [6]

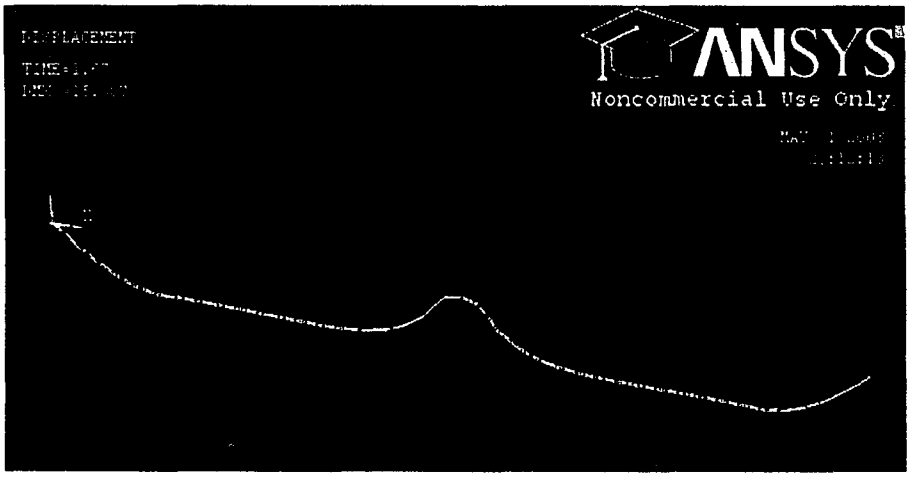

Figure 47: ANSYS Simulation: Sagging, "Wave" Defect Relaxing Out, Time = 1.67 [6]

[illegible] that started with a defect in it. This would simulate what might occur if a "wave" [illegible] in the Enterprise EPO polymer sheets at Ford R&D were to remain trapped in the [illegible] as the mold came into contact with it. [6] The sequence of pictures seen in Figures 36-38 shows the progression of the simulation.

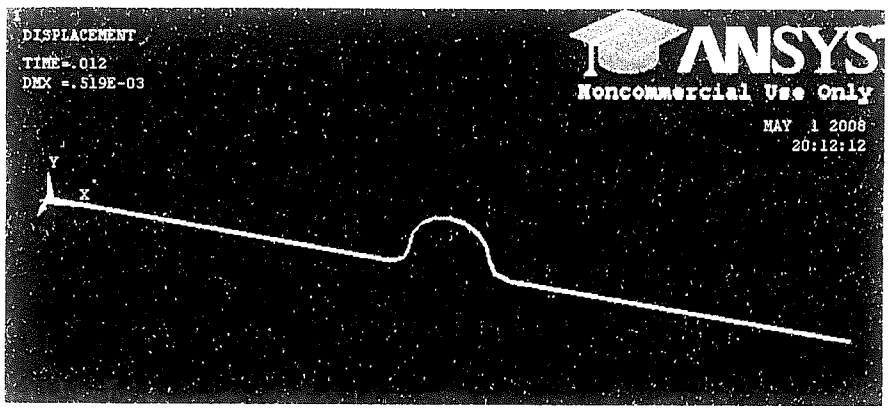

Figure 36 – ANSYS Simulation "Wave" Defect Initially in Sheet, Time = 0.012 [6]

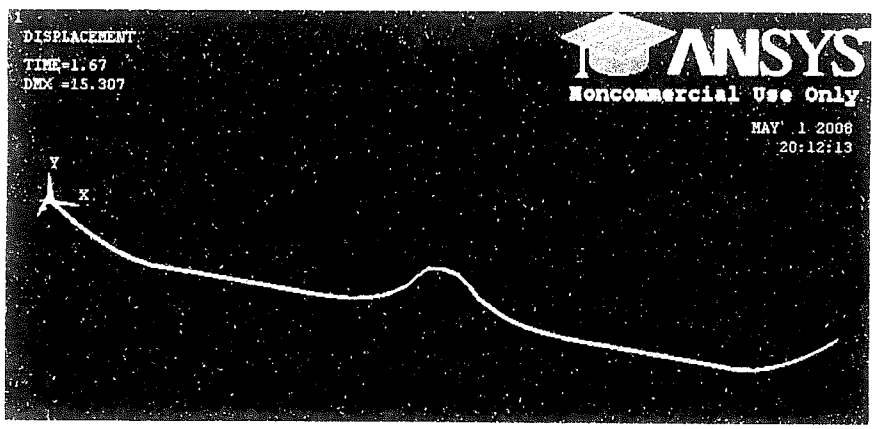

Figure 37 – ANSYS Simulation, Sagging "Wave" Defect Relaxing Out, Time = 1.67 [6]

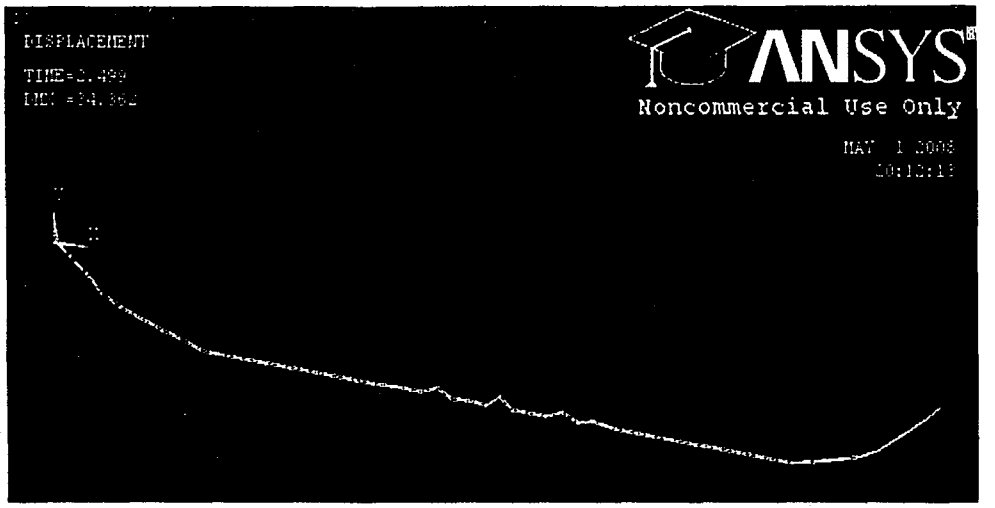

Figure 48: ANSYS Simulation: Sheet in Contact with Flat Plate Defect Trapped in Final Part, Time = 2.499 [6]

The simulation shows that if a defect is initially present in a sheet, like one that may form during the heating process, it could remain trapped in the final product causing a surface defect.

12. Thermoforming Experiments

Since the relatively crude FEM model did not provide any valuable insight into micro defect formation, a controlled experiment was designed to help determine other possible causes of part micro defects. The objective of the experiments would be to trap a defect similar to the one seen on the Ford rocker panel part. Using the thermoformer at Lehigh, a sheet of Schulman 1040E TPO would be inserted into the oven, heated and then formed. Since Ford's setup is on a much larger scale than the one at Lehigh, the dimensions needed to be scaled down in size. Below are the measured dimensions of Ford's formed rocker panel.

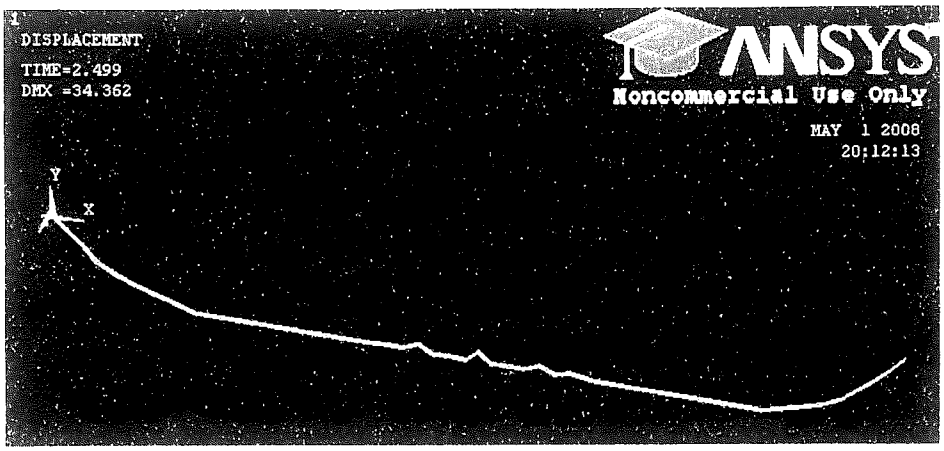

Figure 48: ANSYS Simulation: Sheet in Contact with Flat Plate Defect Trapped in Final Part, Time = 2.499 [6]

The simulation shows that if a defect is initially present in a sheet, like one that may form during the heating process, it could remain trapped in the final product causing a surface defect.

12. Thermoforming Experiments

Since the relatively crude FEM model did not provide any valuable insight into micro defect formation, a controlled experiment was designed to help determine other possible causes of part micro defects. The objective of the experiments would be to trap a defect similar to the one seen on the Ford rocker panel part. Using the thermoformer at Lehigh, a sheet of Schulman 1040F EPO would be inserted into the oven, heated and then formed. Since Ford's setup is on a much larger scale than the one at Lehigh, the dimensions needed to be scaled down in size. Below are the measured dimensions of Ford's formed rocker panel.

Ford Rocker Panel Dimensions in Inches				
	Formed Part	Extra For Clamp	Total	Clearance
Length	46	2	48	2.5
Width	14.5	3	17.5	2.5

Total Aspect Ratio	L/W =	2.742857143
Clamp Aspect Ratio	L/W =	3.172413793

Ford Rocker Panel Dimensions in SI Units (m)				
	Formed Part	Extra For Clamp	Total	Clearance
Length	1.1684	0.0508	1.2192	0.0635
Width	0.3683	0.0762	0.4445	0.0635

Total Aspect Ratio	L/W =	2.742857143
Clamp Aspect Ratio	L/W =	3.172413793

Figure 49: Dimensions of Rocker Panels Formed at Ford R&D

12.1. Initial Design of Experiment

A flat aluminum plate would be installed into the thermoformer's moveable platen. After the TPO sheet was heated properly so it was sagging, the plate would then be driven up into the sheet and no vacuum would be applied. The initial assumption was that since the sheet sags in a parabolic manner, as the plate was elevated into it, the sheet would lay neatly onto the aluminum surface squeezing out trapped and form a relatively smooth flat surface. Conditions would then be modified in an attempt to trap an initial defect that might be observed during initial heating and sag of the thermoplastic sheet.

The Schulman 1040E sheets available at Lehigh measured 30.5" by 20.5" and to properly fit them in the thermoformer they were cut in half widthwise to 30.5" by 10.25". An aluminum plate with dimensions of 26" by 6" was installed on the moveable bottom platen of the thermoformer and the clamps inside the thermoformer were adjusted to be

29.34" long by 9.25" across. These dimensions properly scaled down every component of the thermoforming setup at Ford's laboratory 66%.

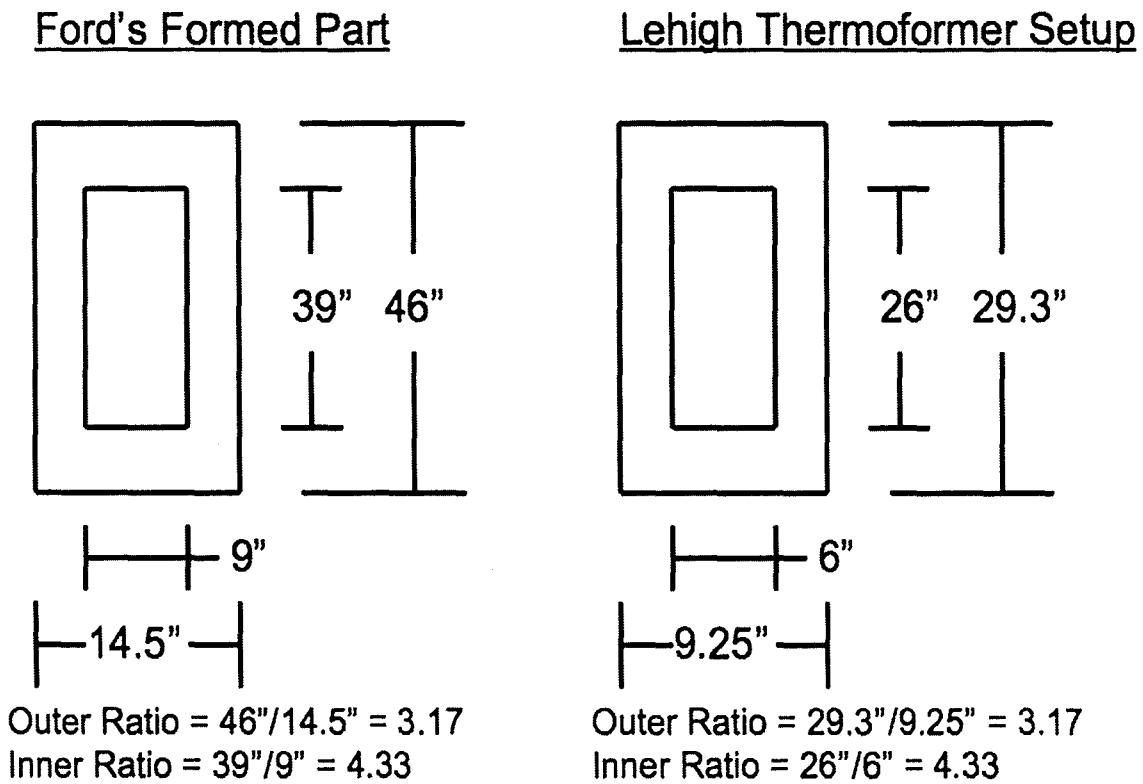

Figure 50: Dimensions and Ratio of Thermoforming Setups

Conveniently, the Schulman 1040E sheet sent to Lehigh was thinner than the actual sheet used at Ford's labs. A Hall-effect gauge was used to make thickness measurements on 10 samples and an average thickness of 1.598 mm was obtained. The undeformed part of the Schulman 1040E sheet, which contained the defect created at Ford R&D, had a thickness measurement of 2.93 mm, thus the Schulman 1040E used in the experiments at Lehigh were 54% thinner.

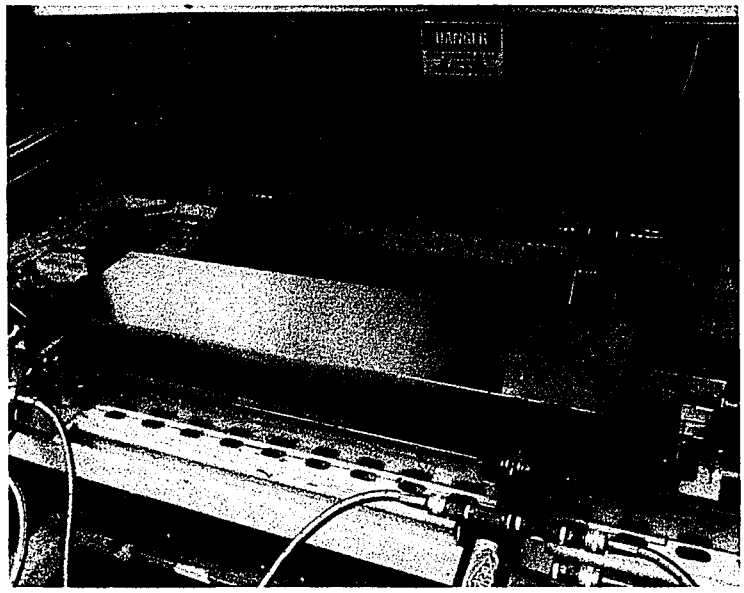

Figure 51: Initial Aluminum Rectangular Plate Thermoforming Setup at Lehigh

A total of 10 experiments were run with the flat aluminum plate setup. After preheating the oven, a sheet of Schulman 1040E TPO was clamped and inserted into the oven. After an average of 2 minutes and 10 seconds, enough time to allow for approximately 3 inches (0.0762 m) of sag, the sheet was moved out of the oven. At this moment, the infrared spot pyrometer gun was aimed at the sheet to obtain a temperature reading in the center, which on average was 215°C. The aluminum plate was then elevated to 3 inches past the initial plane of the TPO sheet. After initial contact the sheet sat neatly on the aluminum plate and the surface looked smooth and completely flat. Interestingly, about 5 seconds after this initial contact, small bubble defects began to form randomly on the plate, as seen in the sequence of images seen in Figures 52-54.

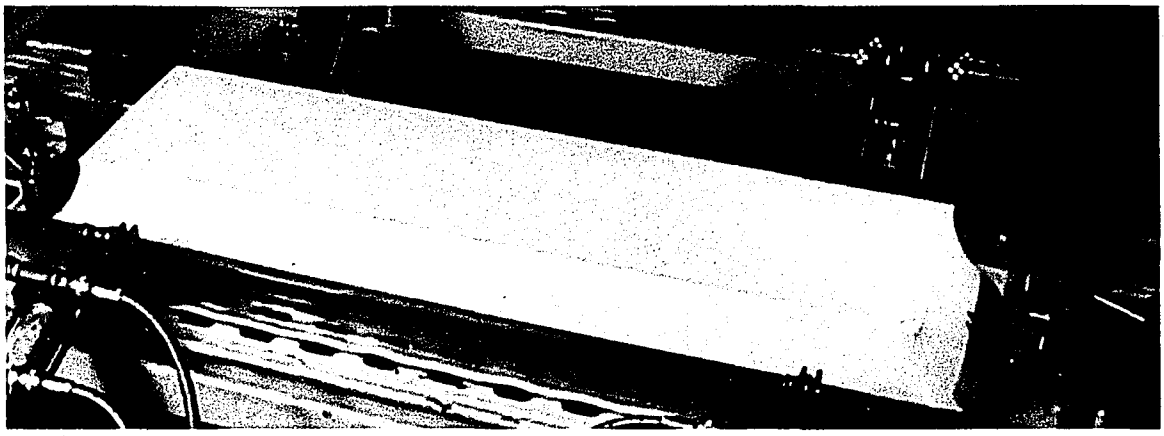

Figure 52: Smooth Sheet Resting on Aluminum Plate Immediately After Contact

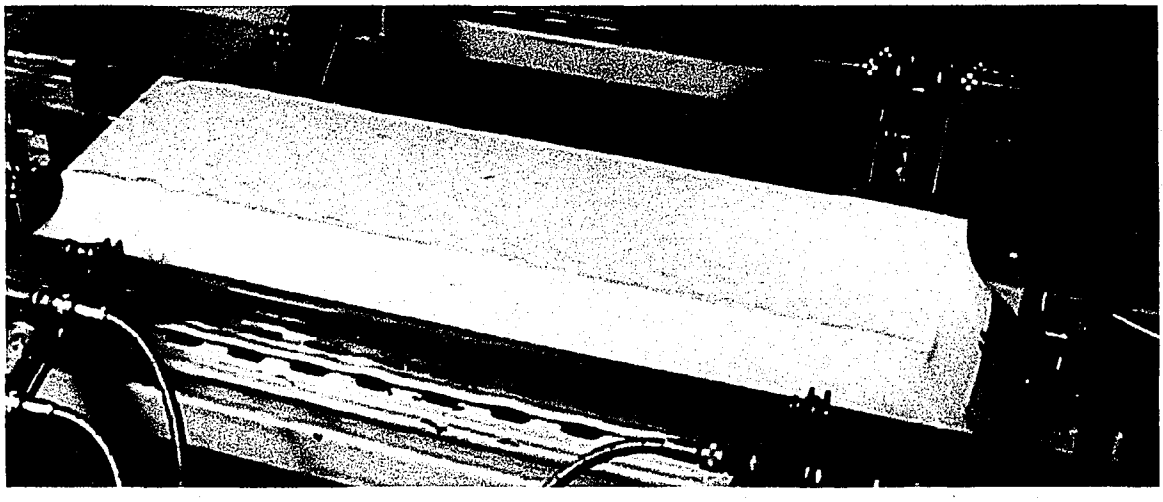

Figure 53: ~5 Seconds After Contact Bubbles Form

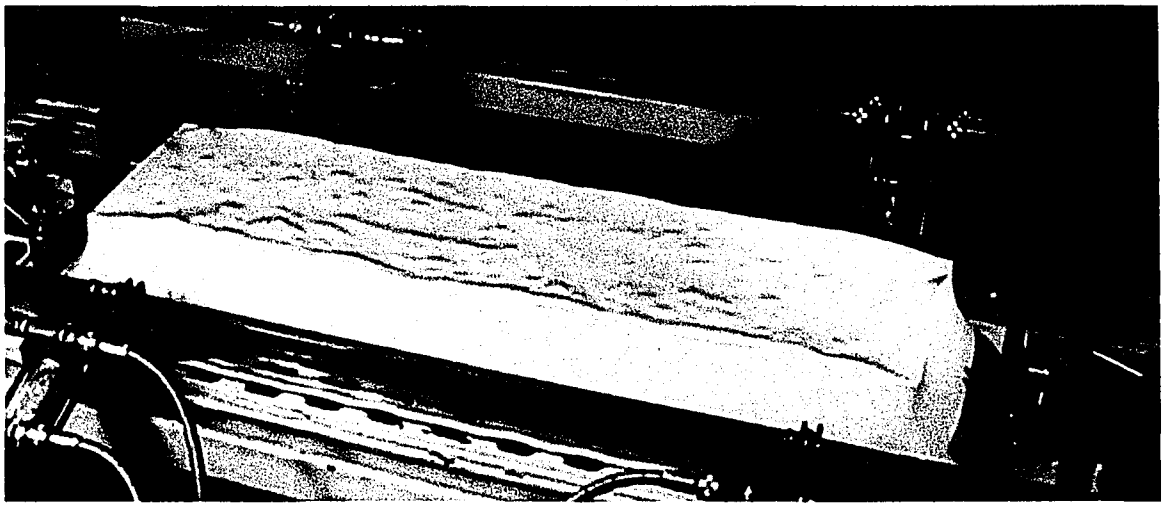

Figure 54: ~20 Seconds After Contact, Bubbles Fully Formed and Set In Part

This bubbling defect was observed on all 10 experiments. It is theorized that a small amount of air becomes trapped between the plastic sheet and the flat mold surface, explaining why the air could not be squeezed out as the polymer contacted the flat surface. Once the trapped air, which is initially at room temperature, contacts the hot plastic (215°C) heat transfer begins to occur raising the trapped air's temperature.

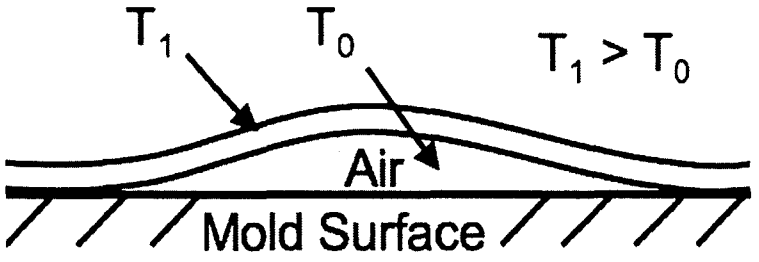

Figure 55: Temperature Difference Between Trapped Air and TPO Sheet

Assuming the air bubble is sealed on all sides due to the sticking of the plastic to the aluminum mold, this creates a constant control volume. With this constant volume, as the temperature of the air rises, the pressure inside must also rise to satisfy the ideal gas law:

$$PV = nRT \tag{17}$$

Where:

P is the pressure of the gas
V is the volume, constant
N is the number of moles of gas, constant
R is the Universal Gas Constant
T is the temperature of the gas

This pressure forces the soft hot plastic to bubble as the plastic is cooling, resulting in the final bubbled shape.

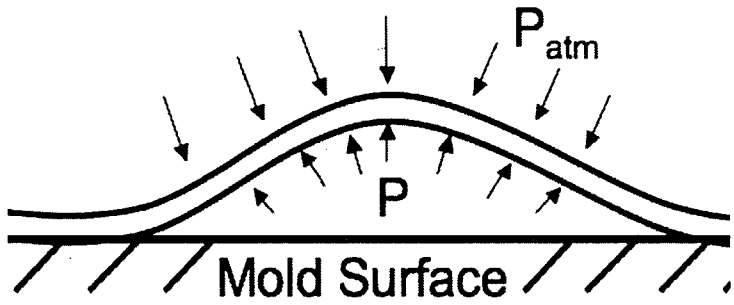

Figure 56: Generated Pressure Due to Increasing Temperature Causes Deformation

The Ideal Gas Equation (17) can be rearranged to calculate an estimated change in pressure leading to the bubble deformations. With the initial air temperature (room temperature), $T_1 = 30°C = 303$ K, the temperature of the sheet, $T_2 = 215°C = 488$ K, $P_1 = P_{atm} = 14.696$ psi, and the volume and number of moles of air constant, the equation becomes:

$$\frac{T_1}{P_1} = \frac{T_2}{P_2} \tag{18}$$

Rearranging to solve for P_2 ...

$$P_2 = \frac{P_1 T_2}{T_1} = \frac{14.696 psi \cdot 488K}{303K} = 23.67 psi \tag{19}$$

Thus the net pressure inside the bubble is:

$$P_{Net\_Inside\_Bubble} = P_2 - P_{atm} = 23.67 - 14.69 = \sim 9 psi \tag{20}$$

If the bubble is then modeled as a hemisphere with radius r, and the thickness at the top of the bubble, t, the stress inside the sheet should be:

$$\sigma_{\theta\theta} \approx \frac{P_{Net} r}{2t} \tag{21}$$

The Hall-effect gauge was again used to take the thickness measurement at the top of formed bubbles and an average thickness was found to be 0.052". A caliper was then

used to estimate the radius of a bubble, which was found to be 0.125". Plugging these values into equation (21):

$$\sigma_{\theta\theta} \approx \frac{P_{Net} r}{2t} = \frac{9 \cdot 0.125}{2 \cdot 0.052} = 10.8 psi \tag{22}$$

Thus a value for stress applied the sheet of 10.8 psi can be estimated.

12.2. Experiments With Vacuum Holes

From the previous experiment, it can be determined that air entrapment must play an important role in defect formation on relatively flat surfaces. In an effort to better understand this phenomena, a second design was created in attempt to compare forming conditions, with different air entrapment. The previous experiment was replicated on a mold of the same dimensions with, vent hole patterns drilled into the aluminum surface to remove trapped air during forming. A vacuum box was constructed on which interchangeable mold plates could be placed. A vent hole was dilled into the bottom for the vacuum line and support beams were placed across the center of the box for added stability.

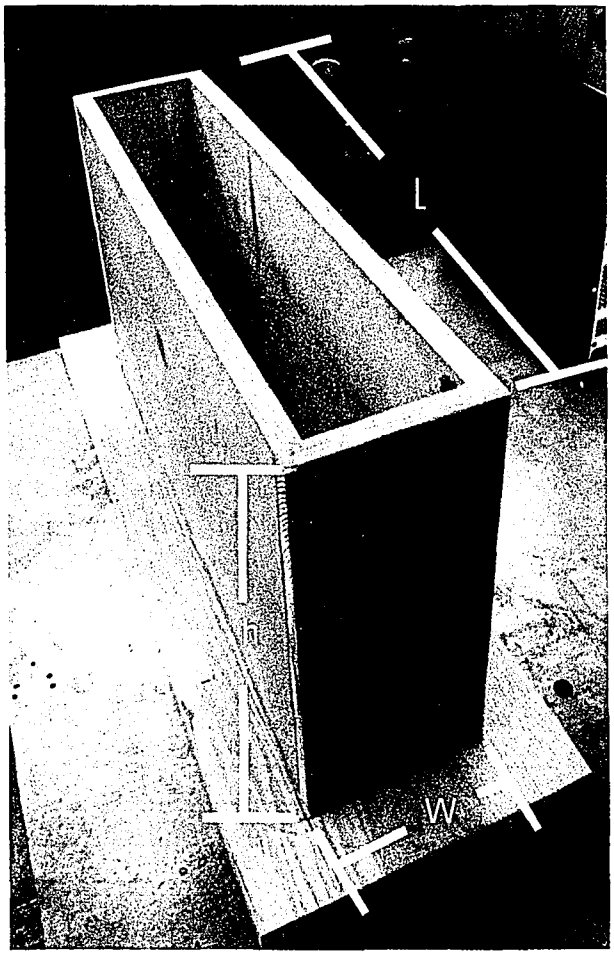

Figure 57: Vacuum Box (Before Stabilizers Were Added)

The box's dimensions measured 26" long by 11" tall by 6" wide, with a large base platform for easy clamping on to the thermoforming machine. An aluminum sheet 26" long by 1/32" tall by 6" wide was selected and screwed onto the top of the vacuum box to act as the mold surface. The 1/32" aluminum sheet thickness provided significant structural stability while still allowing easily repeatable drilling of vent holes.

Calculations to determine the proper number of vent holes were performed. It is recommended that the drill bit used to make vent holes be at maximum half the thickness of the sheet being formed. [2] This prevents the soft thermoplastic sheet from being sucked into the vent holes creating surface defects and possibly damaging the mold. The

Schulman 1040E TPO sheets were 0.0629" (1.598 mm) thick and thus a 1/32" diameter (0.3125", 0.79375 mm) drill bit was used, since it is almost exactly half the 1040E sheet thickness. The method prescribed in Florian's Practical Thermoforming [2] was then implemented to do the calculation which is expressed by the formula (23):

$$N = \frac{P}{U} \div D = \frac{PD}{U} \tag{23}$$

Where:

N = Number of vent holes required per mold unit
P = Cross sectional area of the vacuum piping used
U = Number of individual molds (ups)
D = Drill bit cross sectional area

The table below shows the applicable numbers for Lehigh's system

Florian Method		
Plumbing Pipe Cross Sectional Area, P	0.049	Inches^2
Level Changes "Ups", U	1	
Drill Bit Cross Sectional Area, D	0.000767	Inches^2
N = (P/U)/D	64	Holes

Figure 58: Vent Hole Calculation [2]

A flat mold surface was then created with an objective to see how different vent hole distributions would change observable bubbling defect formation. A border of 0.75" (19.05 mm) on the mold design was left without vent holes, as this is the area where the wooden vacuum box contacts the aluminum plate, and 5 sections with different concentrations was fabricated as shown in Figure 58. Section 1 had 30, section 2 had 21, section 3 had 14, section 4 had 5 and section 5 had 0 vent holes as seen in the picture below, where a blue dot represents a vent hole. A total of 70 vent holes were drilled, which is slightly more than the minimum required 64 (calculated in Figure 58).

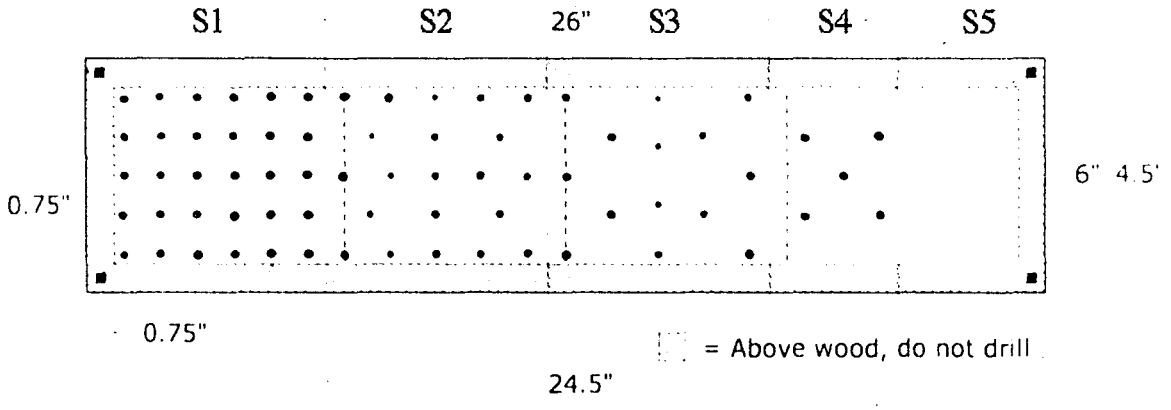

Figure 59: Mold Surface Design with Variable Vent Hole Distribution

Once this mold was installed onto the thermoforming machine 5 experiments were conducted. The sheets were inserted into the oven for an average of 2 minutes and 10 seconds, enough time to allow for approximately 3 inches (0.0762 m) of sag to form. The sheet was extracted from the oven and a temperature reading was taken with the spot IR gun and the same average temperature of 215°C was obtained. The mold was elevated 3 inches past the initial plane of contact with the TPO sheet and then vacuum was applied.

As expected, areas with high concentrations of vent holes showed the least bubbling, sections 1 and 2, and defects began to occur as the vent holes became more sparse, sections 3, 4, and 5. To display this in a more visual manner, a picture of the formed sheet was taken from directly overhead, superimposed over the vent hole pattern image, and scaled to its proper size as see in Figure 60:

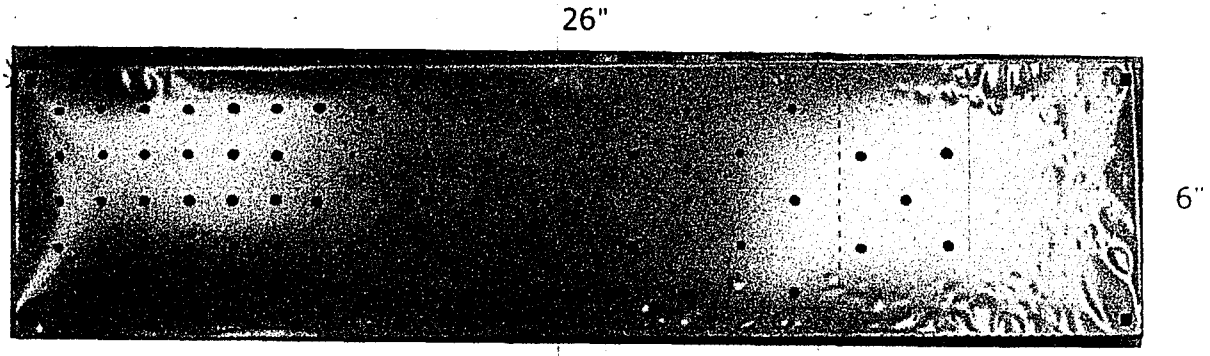

Figure 60: Superimposed Image of Vent Pattern and Formed Part

Figure 58 shows very little to no bubbling in the areas of high vent hole concentration and significant bubbling as the vent holes become less frequent. These results support the theory that miniscule air pockets are being trapped between the mold and the TPO during the forming process. The applied vacuum aided in the evacuation of the trapped air and the effects of the vacuum were most significant in the areas where vent hole concentration was high.

13. Conclusion

The Schulman 1040E formed rocker panel section sample sent to Lehigh had a faintly visible valley defect that was studied with an optical profilometer and proved to be 64.6 μm deep. The defect, although small, was significant enough to prevent the part from having a Class-A surface finish.

The efforts to characterize the Schulman Polytrope® TPP 1040E and Basell Hifax® 756T sheets were valuable in that they showed that two polymers had very similar DSC data but significantly different DMA data. From the DSC tests it was determined the Schulman 1040E had a Melt Onset Temperature of 154.95°C a Peak Melt Temperature of 167.04°C and a Heat of Fusion of 42.39 J/g while the Basell 756T had a

Melt Onset Temperature of 153.1°C a Peak Melt Temperature of 166.4°C and a Heat of Fusion of 39.24 J/g. With these Melt Temperatures so similar it can be concluded that both should be formed around the same temperature range.

More importantly, the DMA tests showed that the Schulman 1040E TPO had a consistently larger Storage Modulus at all temperatures tested as shown in Figure 32: Storage Modulus (E') vs Temperature – Basell 756T and Schulman 1040E.

Thermoforming experiments performed at Lehigh showed that trapped air between the mold and the polymer sheets can cause significant deformations and could be the cause of the defect seen on Ford's Schulman sample. As the trapped air is heated in a constant volume, the heat transferred to that air causes the pressure to rise which results in bubbling. The pressure change calculated was up to ~23 psi (158600 Pa) on the current setup at Lehigh.

The addition of an applied vacuum removed the majority of the air however, some trapped air seemed to be inevitable. It was observed that the area of the sheet that was above the high concentration of vent holes had little to no bubbling, and the area with fewer vent holes exhibited more bubbling.

Relating the differences in material properties of the two polymers to the fact that the Basell 756T consistently experienced less defects [6] than the Schulman 1040E under the same forming conditions, one can draw some interesting conclusions. As with any heated polymer, as it cools with time its modulus increases, but these rates vary from polymer to polymer. If a polymer's modulus increases at a faster rate when cooling it becomes stiffer faster. This higher modulus might be high enough so that the effects of pressure from an air bubble do not impact the final surface quality of a part. Thus a

polymer whose viscoelastic properties are such that its modulus increases at a faster rate when cooled would be desirable, like the case of "Polymer A" shown in Figure 61.

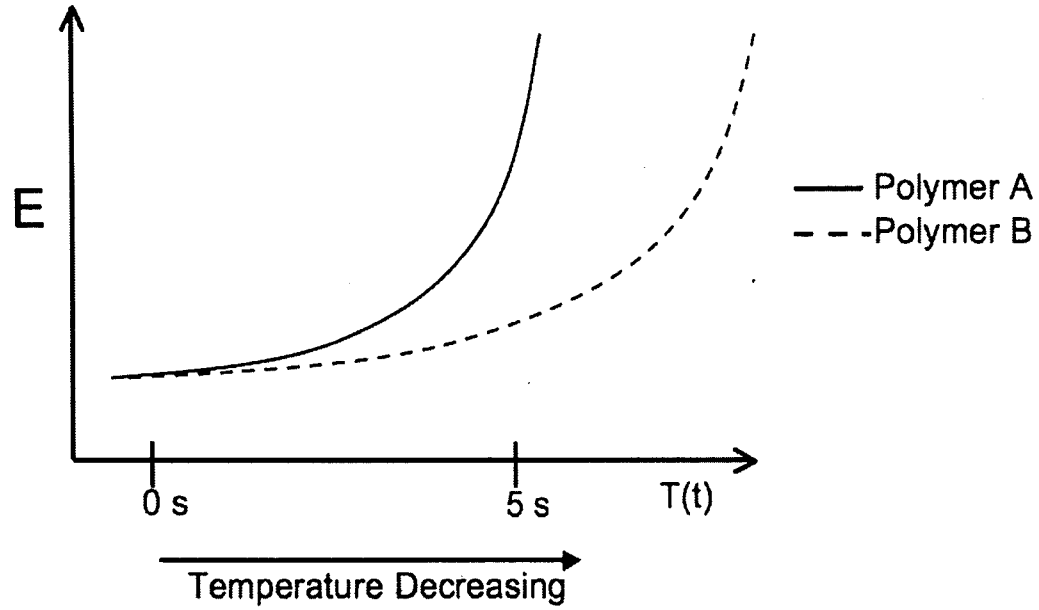

Figure 61: Effect of Decreasing Temperature as a Function of Time on Modulus

Conversely, if the defect is created pre-forming, during initial stages of heating when wrinkling occurs, this type of viscoelastic polymer properties would not be desired. A polymer with a lower modulus as a function of temperature and time would be desired, since the internal stresses would relax out and the defect would dissipate.

The Basell 756T TPO exhibits viscoelastic behavior of a lower modulus as a function of temperature and time when compared to the Schulman 1040E TPO. Given this information and the fact that the Basell 756T consistently thermoformed with less defects than the Schulman 1040E, it is believed that the valley defect seen in the Schulman 1040E rocker panel sample was created during the initial heating stages of the thermoforming process.

It's also possible that there is a coupling between air entrapment and the thermo-viscoelastic behavior during cooling. If one of the "waves" discusses in the section

"Observations of Defect Formation in TPO During Forming," came in contact with the mold surface a long channel plane strain condition would apply.

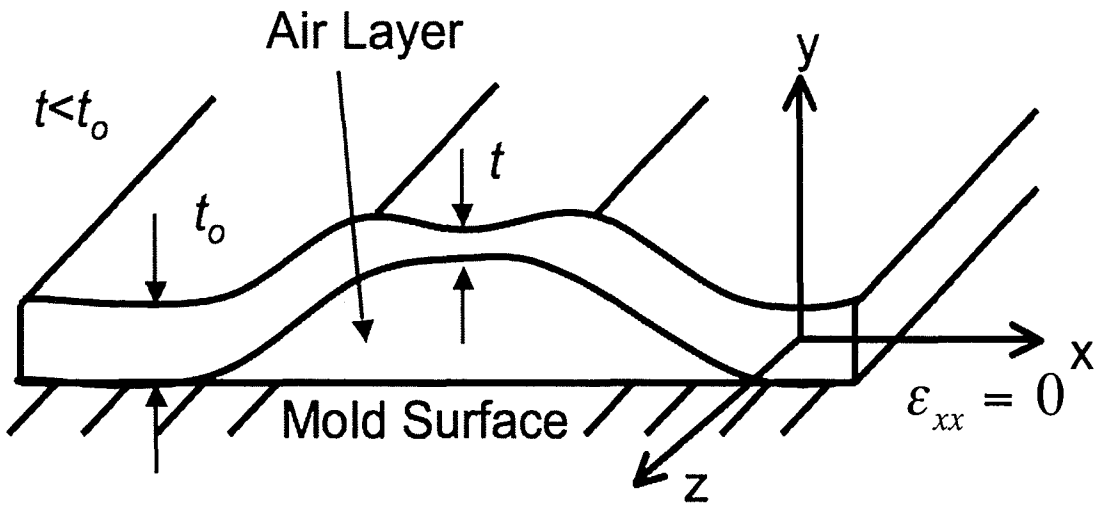

Figure 62: "Wave" Contact with Mold Surface

Surface contact between the plastic and the mold is incomplete because of the air layer causing a channel to develop. As the plastic cools everywhere it is touching the mold, will have no deformation since it is constrained due to no-slip conditions existing. However, the section of plastic above the air bubble does not have a no-slip condition and as it cools, stress will cause it to contract, resulting in the necking effect shown in Figure 62. The thickness above the air layer t, will be smaller than t_o, due to this contraction caused by cooling. For these conditions the following equations can be developed:

For the end constraints:

$$\varepsilon_{xx} = 0 = \frac{1}{E}(\sigma_{xx} - \nu(\sigma_{yy} + \sigma_{zz})) + \alpha\Delta T \tag{24}$$

For long channel plane strain:

$$\varepsilon_{zz} = 0 = \frac{1}{E}(\sigma_{zz} - \nu(\sigma_{xx} + \sigma_{yy})) + \alpha\Delta T \tag{25}$$

With $\sigma_{yy} \cong 0$ for equations (24, 25), the following expressions result:

$$\sigma_{xx} = \sigma_{zz} = -\frac{(1+\nu)}{1-\nu^2} E\alpha\Delta T = -\frac{E}{1-\nu}\alpha\Delta T \tag{26}$$

For -ΔT (cooling)

$$\sigma_{xx} = \sigma_{zz} = \frac{E}{1-\nu}\alpha\Delta T \qquad \text{(Tension)} \tag{27}$$

Then:

$$\varepsilon_{yy} = \frac{1+\nu}{1-\nu}\alpha\Delta T \tag{28}$$

Again assuming an incompressible material, ν=0.5:

$$\varepsilon_{yy} = 3\alpha\Delta T \tag{29}$$

And with:

$$\delta = t - t_o \tag{30}$$

So that:

$$\varepsilon_{yy} = \frac{\delta}{t_o} = \frac{t - t_o}{t_o} = 3\alpha\Delta T \tag{31}$$

And again for -ΔT (cooling):

$$\frac{t}{t_o} = 1 - 3\alpha\Delta T \tag{32}$$

Equation (32) shows that for elastic behavior, thinning does not strongly depend on elastic properties ($0.4 < \nu < 0.5$), but does depend heavily on coefficient of thermal expansion.

14. Future Work

A factor that could greatly contribute to the surface finish quality of thermoformed sheets is the surface roughness of the mold. If air bubbles are being trapped between the mold and the polymer sheet, then a roughened mold surface could be desirable. Roughening the mold surface could create channels on the order of microns through which air could travel to a vent hole. Thus, instead of having a sealed bubble of air which is forced to apply a pressure onto the plastic, the air could escape out a channel preventing a defect from forming. However, too much surface roughness could have an adverse effect. "Olefins tend to alternately slip and stick when vacuum formed. This causes visible ridges in the part surface. These are sometimes wrongly attributed to plug mark-off. Roughening the mold surface does little to prevent sliding and may aggravate the problem."[1] In the future, experiments should be performed to quantitatively investigate this idea and see if there is a amount of roughness that is "just right" to allow trapped air to move to a vacuum hole while preventing ridges from slippage.

As shown in equation (32), thinning behavior in a long channel depend heavily on the coefficient of thermal expansion. Other future work could involve experiments comparing the coefficients of thermal expansion between the Basell 756T and the Schulman 1040E, as this could be playing a large role in the difference in thermoforming behavior of the two materials.

References:

[1] Throne, James L., Technology of Thermoforming, Hanser, New York (1937).
[2] Florian, John., Practical Thermoforming, 2nd Edition, Marcel Dekker, New York (1996).
[3] Williams, M. L., "Engineering Analysis of Viscoelastic Media", Graduate Aeronautical Laboratories California Institute of Technology, Pasadena California (1965).
[4] TA Instruments, "DSC 2920 Differential Scanning Calorimeter Operator's Manual", TA Instruments, New Castle DE (1995).
[5] TA Instruments, "DMA 2980 Dynamic Mechanical Analyzer Operator's Manual", TA Instruments, New Castle DE (1997).
[6] Bekisli, Burak, Technical Report 08.28.2007, Lehigh University, Bethlehem PA (2007).
[7] Plastics Custom Research Services, "The Industrial Thermoforming Business: Review and Outlook", Advance NC (2004).
[8] Sciences etTechniques Industrielle de la Lumiere, Aix en Provence France (2004).
[9] Aloisio, C. J. and Brockway, G. S., "DMA Viscoelastic Analysis of Two Cross-Linked And One Thermoplastic Rubber", ANTEC 2003, pp. 3633-3637.
[10] ANSYS ED 10, "User's Manual: 9.4 Viscoelastic Material Curve Fitting", Cannonsburg PA (2008).
[11] A. Schulman Co., "TPP 1040E Data Sheet", Akron OH (2007).
[12] Basell Co., "Hifax TBC 756T Data Sheet", Hoofddorp Neatherlands (2007).
[13] Utracki, L.A., Polymer Blends Handbook, Vol 1-2, Springer – Verlag (2002).

Vita:

Jonathan Marmillo, son of Gerald and Mary Ann Marmillo, was born on November 5th 1984 and raised in Clifton Park, New York. He attended The Albany Academy for Boys for high school and then matriculated to Lehigh University where he obtained his Bachelor of Science in Mechanical Engineering with High Honors in May 2007. While there he was elected into the engineering honor society Tau Beta Pi, the international mechanical engineering honor society Pi Tau Sigma, and is a member of Pi Eta Sigma national honor society and the National Society of Collegiate Scholars. After receiving his undergraduate degree he stayed at Lehigh University to continue his education and will be receiving his Master of Science in Mechanical Engineering in December 2008. In January he will begin working for General Electric's Energy division in their Commercial Leadership Program.

END OF TITLE